Spring 2015

The Relationship between Volatiles (CO2, H2O, F, S & Cl) and Noble Gases in Reykjanes Peninsula Lavas, Iceland

Lorne Loudin
University of New Hampshire, Durham

THE RELATIONSHIP BETWEEN VOLATILES (CO_2, H_2O, F, S & Cl) AND NOBLE GASES IN REYKJANES PENINSULA LAVAS, ICELAND

BY

LORNE C. LOUDIN

B.S. Keene State College, 2008

THESIS

Submitted to the University of New Hampshire

in Partial Fulfillment of

the Requirements for the Degree of

Master of Science

In

Earth Sciences

May, 2015

This thesis has been examined and approved in partial fulfillment of the requirements for the degree of Master of Science in Earth Sciences by:

Thesis Director, Samuel B. Mukasa
Dean, College of Engineering and Physical Sciences,
Professor of Geology

Julia G. Bryce
Associate Professor of Earth Sciences

Joseph M. Licciardi
Associate Professor of Earth Sciences

On January, 22 2015

Original approval signatures are on file with the University of New Hampshire Graduate School.

DEDICATION

This thesis is dedicated to all of my family, my mom and dad, Mike Muntz, Tim Donovan, and especially Mamaw. Thank you all for your support.

ACKNOWLEDGEMENTS

I would like to express my deepest gratitude to all of those who have assisted and supported me in completing this body of work. First, I would like to thank my advisor, Dr. Samuel B. Mukasa, for inspiring and assisting me in carrying out this project. He dedicated his resources and time, and engaged me in valuable discussions on the topic. In addition, Dr. Mukasa provided me with field opportunities, introducing me to a world of scientific experiences. I would also like to thank the members of my thesis committee, Drs. Julia G. Bryce and Joe Licciardi. Many thanks to Dr. Julia G. Bryce for supporting me through the entirety of this master's degree program, always willing to discuss, assist, train, and support me in all things scientific. A most sincere thanks to Dr. Joe Licciardi for imparting his expertise concerning noble gases and Iceland geology.

My appreciation extends to the Department of Earth Sciences at the University of New Hampshire and to all the professors who challenged me. To all of the postdocs, and visiting scientists who supported and encouraged me, sharing their knowledge and expertise, I am grateful. Specifically, Drs. Martin Guitreau, Pier Paolo Giacomoni, and Joan Cabato who eagerly and energetically shared their knowledge, skills, and ideas with me. I would also like to thank my colleague Kim Aviado for her support and generosity with assisting me in the laboratory.

The following individuals and laboratories were most valuable in providing analytical and data processing support. First and foremost, Brian Monteleone and Nobu Shimizu at the Northeast National Ion Microprobe Facility of the Woods Hole Oceanographic Institute, thank you for assisting me with volatile data acquisition and processing. Bruce Watson, Dustin Trail and their team in the Piston Cylinder Laboratory at Rensselaer Polytechnic Institute, provided support and

information regarding high-pressure, melt-inclusion homogenization experiments. I would also like to thank Nilanjan Chatterjee at the Massachusetts Institute of Technology Electron Mircroprobe Facility for assistance with some analytical work.

This research was made possible by the support of start-up funds to Dr. Samuel B. Mukasa. A Research Assistantship was provided to me by Samuel B. Mukasa, and supported in part by National Science Foundation grant EAR-1321633. In addition, the Department of Earth Sciences provided me with a Teaching Assistantship, which helped to support this research.

TABLE OF CONTENTS

LIST OF FIGURES

LIST OF TABLES

ABSTRACT

THE RELATIONSHIP BETWEEN VOLATILES (CO_2, H_2O, F, S & Cl) AND NOBLE GASES IN REYKJANES PENINSULA LAVAS, ICELAND

by

Lorne C. Loudin

University of New Hampshire, May, 2015

The presence of volatiles in the local mantle magma source region has been suggested as a contributor to the observed high melt production rates in the volcanic segments of the island of Iceland. However, the source of volatiles beneath this island remains enigmatic. New volatile (CO_2, H_2O, F, S and Cl) concentration data for 157 olivine-hosted melt inclusions in concert with noble gas data (He and Ne) from the Reykjanes Peninsula, Iceland, allow for the reconstruction of magma degassing and the distribution of volatiles in the mantle beneath Iceland. Water concentrations in olivine-hosted melt inclusions from this study record a maximum H_2O concentration of 1.99 ± 0.06 wt. %. The H_2O concentrations are not correlated with any of the major oxides, but are in some cases elevated relative to other incompatible elements. Solubility models we have tested show that olivine-hosted melt inclusions from the Reykjanes Peninsula have considerably less CO_2 for the observed H_2O, which implicates degassing to be a more important volatile-loss process than diffusion. Volatile concentrations are negatively correlated with R/R_a, a relationship that implies lower H_2O concentrations in the primitive high-^3He mantle

component and higher-water concentrations in samples that approach Mid Ocean Ridge Basalt (MORB) R/R_a values. Water concentrations are highest along the atmosphere-MORB mixing line on a three-neon isotopic plot, and primitive samples plotting along the atmosphere-solar mixing line have lower water concentrations. These relationships suggest that a volatile-enriched recycled component with high H_2O and low $^3He/^4He$ values has mixed with a primitive mantle component that is low in H_2O but has high $^3He/^4He$ values. These two end-member compositions are consistent with a plume component and a depleted MORB source component – potentially enriched and fluxed by subducted components – mixing in the mantle beneath Iceland, and melting to produce the observed volcanic products. These findings support previous suggestions for a three-component-mixing model to explain the relationship between He and H_2O in Reykjanes Ridge lavas.

1. INTRODUCTION

Analyses of volcanic glasses and olivine-hosted melt inclusions from ocean-island basalts (OIBs) and mid-ocean ridge basalts (MORBs) have demonstrated that OIB are enriched in volatiles (CO_2, H_2O, F, S, and Cl) relative to MORB (e.g., Moore, 1965; Moore et al., 1982; Poreda et al., 1986, Dixon et al., 1991, Dixon et al., 1997; Hauri et al., 2002; Nichols et al., 2002; Métrich et al., 2014). These and related findings suggest that volcanism associated with mantle plumes may in some cases be aided by the presence of volatiles in the mantle as opposed to the singular presence of a thermal anomaly or rapid decompression (e.g., Schilling et al., 1980; Nichols et al., 2002; Metrich et al., 2014). However, as noted by Dixon and Clague (2001), simply knowing that OIBs are enriched in volatiles relative to MORB does not provide us with deep insight into the source of volatiles. It is through assessing the relationship volatiles have with noble gases and incompatible elements that we gain valuable insight into their source.

In this study I elucidate the origin of volatiles in olivine-hosted melt inclusions from the Reykjanes Peninsula, Iceland, and evaluate the role of a recycled crustal component as the source of volatiles in the mantle beneath the island. I present new volatile data derived from splits of rock from the same suite of samples used in earlier studies (Dixon et al., 2000; Dixon 2003), which used He and Ne isotopic data to argue for magma generation by binary mixing between a less depleted mantle domain, containing vestiges of primordial He and Ne, and the more highly depleted MORB mantle beneath Iceland. Together with the noble gas data, the new volatile concentrations presented here provide new insight into the origin of volatiles in Icelandic magmas and elucidate the role of recycled oceanic lithosphere in generating the Iceland plume. The notion

that subducted lithosphere may play an important role in generation of ocean-island magmas was first suggested by Hoffmann and White (1982) examining other localities. The results presented here confirm the applicability of that model in Iceland and allow for an enhanced understanding of how this recycled oceanic lithosphere is interwoven in the MORB source region.

The importance of H_2O in the generation of MORB and OIB is nontrivial. Water in the mantle lowers the solidus substantially, increasing melt production at a given temperature (Kushiro et al., 1968; Hirose and Kawamoto, 1995; Gaetani and Grove, 1998), and allowing melting to commence at higher pressures (McKenzie 1985; Robinson et al., 2001). Moreover, Asimow and Langmuir (2003) showed that an excess of H_2O in OIB and MORB increases melt production but lowers the total volume of melting when it is the sole factor. They demonstrated that the effect of H_2O on the extent of melting is significant not only in regions of anomalously high-water concentrations, but also in MORB with the average H_2O content of ~0.2 wt. %. Consequently, these processes have important implications for the major- and trace-element chemistry of mantle-derived magmas.

Some volatile studies suggest that plumes originating from less depleted domains within the lower mantle generally contain higher water concentrations than plumes demonstrably originating from recycled lithosphere in the shallow mantle (Jambon and Zimmerman, 1990; Dixon et al., 1997; Dixon and Clague, 2001; Dixon et al., 2002). Dixon et al. (2002) attributed the difference in H_2O concentrations between the two plume sources to the dehydration of recycled lithosphere during subduction and argue that subduction could remove ~97% of the H_2O from the down-going slab and accordingly cause plumes originating from recycled lithosphere to be "damp" not "wet" (Dixon et al., 2002).

Conversely, a recent investigation of volcanic glasses from the Manus Basin demonstrated that if H_2O and H isotope anomalies are correlated to the seismic anomaly beneath the basin, significant amounts of H_2O are potentially transferred into the mantle and preserved for up to 10^9 years (Shaw et al. 2012). In an investigation of tholeiitic glass from the Azores, Schilling et al. (1980) proposed that "hot spots" in the North Atlantic were possibly "Wet Spots" undergoing volatile induced flux melting. The concept of wet recycled material in plumes was later applied to the ridge sections near Iceland by Poreda et al. (1986) based on the relationship between H_2O and He isotopes in the Reykjanes, Kolbeinsey, and Mohns ridges. These findings resulted in the hypothesis that three-component mixing involving two plume components and depleted MORB occurred beneath the region.

In the three-component model, the two plume components included a domain with high $^3He/^4He$ and low H_2O, and a domain containing recycled material with low $^3He/^4He$ and high H_2O (Poreda et al., 1986), contradicting the model of Dixon et al. (2002) that suggests low H_2O in the recycled component. In the model presented by Poreda et al. (1986), the Reykjanes Ridge segment was believed to involve only the less-depleted plume component and the depleted MORB source (Poreda et al., 1986). However, with additional arguments, mainly H_2O/Ce, Michael (1995) included the recycled component, with high H_2O and low $^3He/^4He$, beneath the Reykjanes Ridge, invoking rapid subduction as a cause for the H_2O anomaly. Two-component-mixing models have also been suggested to explain heterogeneity in Icelandic magmas. The two-component models invoke a pyroxenite-peridotite mantle and require a depleted MORB source and an enriched recycled component (Shorttle and Maclennan 2011; Koornneef et al., 2012).

Iceland is the ideal location to investigate the origin of volatiles in a hybrid volcanic setting because it represents the interaction of a mantle plume and a major spreading center, the Mid-

Atlantic Ridge (Schilling, 1973; Wolfe et al., 1997). On the basis of noble gas studies, it is generally accepted that binary mixing between a plume component and MORB component occurs beneath Iceland, and particularly beneath the Reykjanes Peninsula (Moreira et al., 2001; Dixon, 2003; Furi et al., 2010). Water and other volatile concentrations increase along the MAR towards the Iceland plume (Schilling et al., 1983; Poreda et al., 1986; Hilton et al., 2000; Nichols et al., 2002). In addition, Nichols et al. (2002) proposed that the mantle source beneath Iceland is enriched in H_2O (e.g., ~620-920 ppm) relative to the MORB source ~110 ppm (Workman and Hart, 2005). The H_2O content of the Iceland plume estimated by Nichols et al. (2002) spans the HIMU and FOZO mantle endmember H_2O compositions proposed by Dixon et al. (2002). However, the source of volatiles remains enigmatic.

As noted by Sigmarrsson and Steinthorsson (2007), the possibility of ancient recycled oceanic lithosphere in the mantle beneath Iceland is an important consideration when investigating mantle plume heterogeneity beneath the island and has been proposed on the basis of radiogenic isotopes and trace elements by several authors (Chauvel and Hemond, 2000; Skovgaard et al., 2001; Breddam, 2002; Stracke et al., 2003a; 2003b; Kokfelt et al., 2006; Brandon et al., 2007; Sobolev et al., 2008; Koornneef et al., 2012). Owing to the relationship between trace elements and Pb-Nd-Sr-O isotopes, the subduction of an entire section of oceanic crust was proposed to explain both enriched and depleted plume components beneath Iceland (Chauvel and Hemond, 2000; Kokfelt et al. 2006). Kokfelt et al. (2006) suggested that radiogenic Pb coupled with trace-element patterns in alkali basalts from Iceland were similar to the HIMU mantle component beneath St. Helena and that these basalts represented the enriched source, derived from recycling the upper, hydrothermally altered oceanic crust. However, unradiogenic Pb, coupled with geochemical anomalies unique to the MORB source, defined the depleted component resulting

from recycling of gabbroic and ultramafic cumulates in the lower oceanic crust (Kokfelt et al., 2006). Further evidence for younger recycled crust being superimposed on primitive high $^{3}He/^{4}He$ mantle near the core-mantle boundary is suggested by relationships between $^{187}Os/^{188}Os$ and $^{3}He/^{4}He$ coupled with solar Ne (Brendon et al., 2007). The age of recycled crust incorporated into the mantle beneath Iceland has been constrained to ~1-2 Ga (Kokfelt et al., 2006; Brandon et al., 2007; Sobolev et al., 2008).

The new volatile data presented here record H_2O concentrations in Reykjanes Peninsula melt inclusions as high as 1.99 ± 0.06 wt. %. The volatile data are evaluated in terms of mixing between an enriched plume component and the depleted MORB mantle, and in terms of recycled oceanic lithosphere mixing with the less depleted mantle to generate two unique plume components beneath Iceland.

I propose that the volatile concentrations of Reykjanes Peninsula melt inclusions are best explained by mixing an ancient recycled component with the ambient MORB mantle. This model is in agreement with the three-component-mixing model proposed by Poreda et al. (1986) and Michael et al. (1995), and it does not rule out a two-component model involving the presence of a pyroxenite-peridotite mantle already modified by an influx of subduction components (Shorttle and Maclennan 2011; Koornneef et al., 2012). For the paleo-position of the mantle beneath the Iceland region, emplacement and subsequent mixing of recycled oceanic lithosphere into the less differentiated mantle can be explained by subduction during the Ketilidian Orogeny (1.85-1.72 Ga) of south Greenland (Garde et al., 2002). The timing of the Ketilidian Orogeny is consistent with three independent age models that constrain recycled material in the mantle beneath Iceland to a range of ~1-2 Ga (Kokfelt et al., 2006; Brandon et al., 2007; Sobolev et al., 2008).

2. GEOLOGICAL SETTING AND SAMPLE SELECTION

Iceland coincides with the Mid-Atlantic Ridge where anomalously high volcanic outpourings and formation of crust are attributed to the upwelling of a mantle plume whose hotspot is currently located beneath Vatnajökull Glacier (Figure 1A; Schilling, 1973; Wolfe et al., 1997). This hotspot is presumed to have traversed Iceland in an accommodation zone between the Snæfellsnes Peninsula in the west and its current location beneath Vatnajökull glacier to the east (Figure 1A), as the North American Plate has moved westwards. Active upwelling has caused crustal thicknesses beneath Iceland to exceed typical ocean crust values (White, 1997), reaching a maximum thickness of ~40 km near the locus of plume activity contrasting to ~15 km south of the Reykjanes Peninsula (Darbyshire et al., 2000).

The Reykjanes Peninsula in southwest Iceland (Figure 1A) is part of the neovolcanic zone, a continuation of the MAR and an active rift zone dominated by tholeiitic volcanism (Jakobsson et al., 1978). Igneous basement rocks of the Reykjanes Peninsula are younger than 700 ka (Peate et al., 2009). Five en-echelon volcanic systems characterized by a central volcano and fissure swarm make up the Reykjanes Peninsula (Figure 1B; Jakobsson et al., 1978; Peate et al., 2009); and volcanic activity in these zones is primarily post-glacial, less than ~15-13 ka (Ingolfsson et al., 1997; Norðdahl and Pétursson 2005; Geirsdóttir et al., 2009) From southwest to northeast the volcanic systems of the Reykjanes Peninsula are the Reykjanes, Grindavík, Krýsuvík, Bláfjöll, and the Hengíll swarms (Figure 1B; Jakobsson et al., 1978; Peate et al., 2009). The Reykjanes Peninsula is bound to the northeast by the Hengíll swarm (Figure 1B), which sits at a triple junction

between the Reykjanes Peninsula, the Western Volcanic Zone, and the South Iceland Seismic Zone (Ferk and Leonhardt, 2009; Einarsson, 2012).

The Hengíll swarm continues to the north forming the WVZ (Peate et al., 2009). Intraglacial volcanism in the neovolcanic zone, including the Reykjanes Peninsula, resulted in the formation of table mountains, or tuyas, flat topped mountains composed of hyaloclastites, pillow lava, and a capping lava (Jakobsson and Johnson, 2012); these are the products of subglacial eruptions penetrating through an ice sheet (Mathews 1947; Licciardi et al., 2007). The volcanic rocks of the Reykjanes Peninsula record the relationship between volcanism and deglaciation (Jakobsson et al., 1978) and show that eruption rates increased by up to ~50 times during the deglaciation of the Reykjanes Peninsula, ~14.5 kyr BP, continuing for ~2-3 ky into the early post-glacial period (Jull and McKenzie, 1996; Maclennan et al., 2002).

The olivine-hosted melt inclusions analyzed in this study are from intraglacial and post-glacial olivine tholeiite and picritic basalts collected from localities on the Reykjanes Peninsula (Figure 1, Table 1) for the noble gas studies of Dixon et al. (2000) and Dixon (2003). Figure 1B shows the studied lava-flow locations and their corresponding volcanic swarms along the Reykjanes Peninsula. The picrites and olivine tholeiites from the WVZ are amongst the least evolved rocks on Iceland with MgO = ~ 8.5 - 14 wt. % (Jakobsson and Johnson 2012). The petrology and mineralogy of Reykjanes Peninsula samples have been described in detail elsewhere (e.g., Jakobsson et al., 1978; Risku-Norja, 1985; Tronnes, 1990; Einarsson, 2012), but in general the samples selected for this study have phenocrysts of olivine, spinel ± plagioclase ± clinopyroxene (Dixon et al., 2000). In addition, these samples record a range of He and Ne isotopic compositions interpreted to represent binary mixing between a plume and MORB end member (Dixon 2003; Table 2). The variations in noble gas signatures and their primitive magmatic

compositions, make these samples well suited for investigating the origin of volatiles in the mantle beneath Iceland.

Mælifell, Miðfell, and Sandfell, are intraglacial, late Pleistocene, hyaloclastite ridges located in the Hengíll swarm (Einarsson, 2012). The Miðfell samples were collected from the southern end of the volcanic edifice (Dixon, 2000) in the Dagmàlafell. The picritic pillow lavas from Dagmàlafell occur in the upper volcanic sequence and are the result of a subglacial fissure eruption (Guerenko and Sobolev, 2006). Plagioclase, Cr-Al-diopside, olivine, and gabroic nodules are abundant in picritic lavas from Miðfell, and sample *Ice-9* is from a locality where gabbroic nodules are present (Dixon et al., 2000). Mælifell is composed primarily of picritic pillow basalts containing Cr-Al-diopside gabbroic nodules (Einarsson, 2012). The Bleikholl sample is an olivine-tholeiite, and the location is characterized by late glacial lava flows outpouring from a crater row (Vargas, 1992). Stora-Eldborg, is located in the Krýsuvík volcanic system and is a post-glacial lava flow containing abundant porphyritic olivine with negligible contents of other phenocrysts (Vargas, 1992).

Olivine grains for this study were selected from a sample suite with known He and Ne isotopic signatures (Table 2). The selected samples represent a range of He and Ne isotopic compositions, suggesting various contributions from plume and MORB end-members (Dixon et al., 2000; Dixon, 2003). The picrite and olivine-tholeiites originally sampled by Dixon et al. (2000) and Dixon (2003) are primitive (MgO = ~ 8.5 -14 wt. %; Jakobsson and Johnson 2012), representing the least evolved rock types on Iceland (Table 1), with high olivine content making them ideal targets for trapped noble gasses. Their primitive composition and high olivine content makes them equally suited for studying volatile concentrations because the trapped melt inclusions should record primary melts representative of their mantle source.

Dixon et al. (2000) and Dixon (2003) showed that samples from Miðfell (*Ice-1b*), Sandfell *(Ice-2),* Stora-Eldborg *(Ice-16),* and Bleikholl *(Ice-25)* contain Ne with isotopic ratios indistinguishable ($\leq 2\sigma$) from the MORB correlation line on a three-Ne-isotope plot. However, additional samples from Miðfell *(Ice-1a and 9)*, fall close ($<1\sigma$) to the air-solar mixing trend, indicating that the Icelandic plume is heterogeneous and contains vestiges of primordial solar neon (Dixon et al., 2000; Dixon, 2003). The Mælifell sample *(Ice-10)* contains Ne that is indistinguishable from the atmospheric isotopic composition for this noble gas (Dixon, 2003). The $^{3}He/^{4}He$ (R/R_a) values measured previously by Dixon et al. (2000) and Dixon (2003) on the olivine grain populations used in this volatile study range from 11±1 to 29±3. These samples represent the noble gas heterogeneity of the mantle beneath Iceland (Table 2), both the primitive He and primordial Ne components, and the MORB-like component, making them well-suited for determining the source of volatiles in Reykjanes Peninsula lavas.

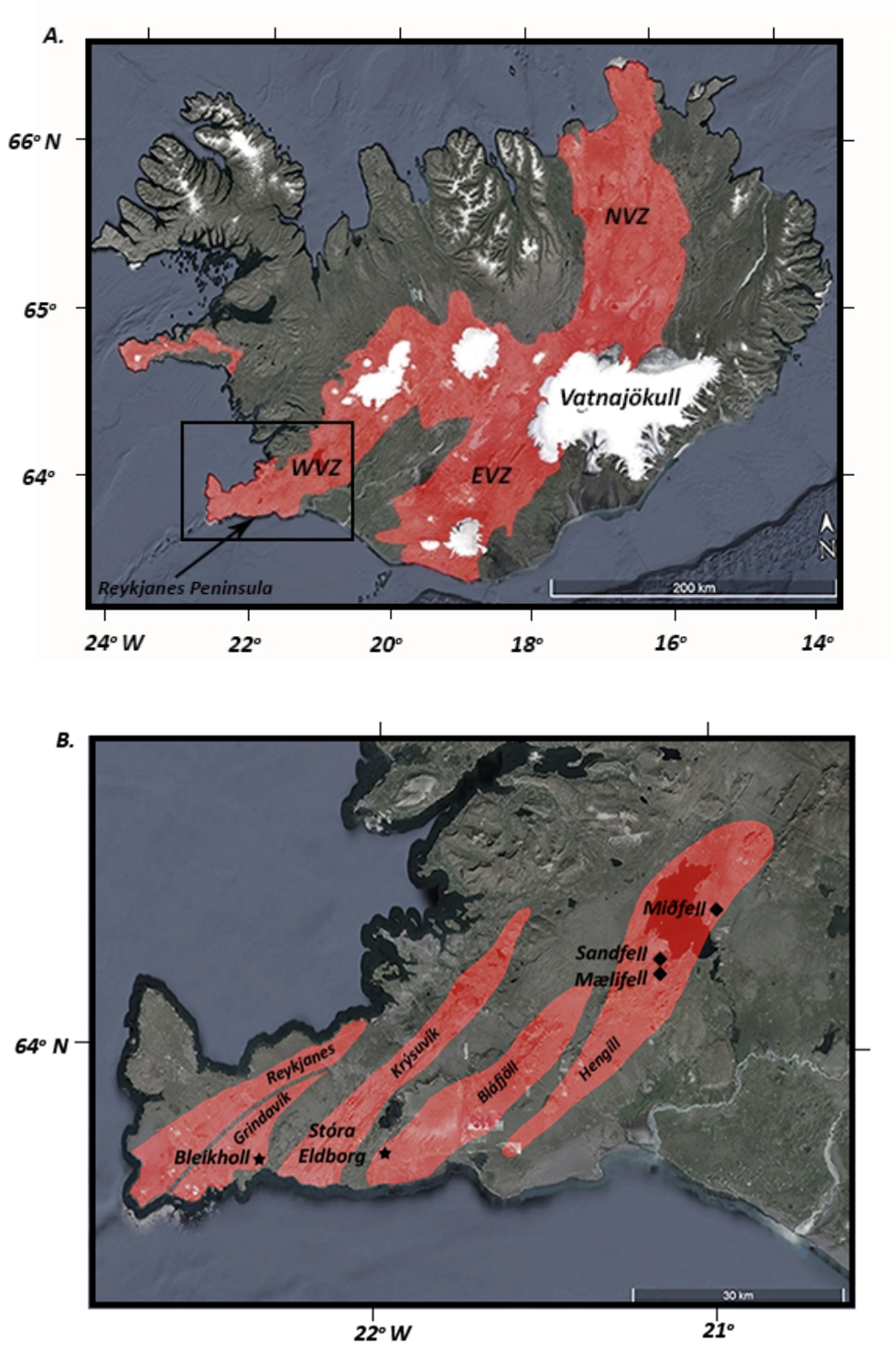

Figure 1: **(A)** Map of Iceland. Samples studied are from the Reykjanes Peninsula (enclosed region). Plume head is located beneath the Vatnajökull glacier. Red zones indicate the neovolcanic zones. WVZ – Western volcanic Zone. EVZ – Eastern volcanic zone. NVZ – Northern Volcanic Zone. **(B)** Location of lava flows studied. Red zones indicate volcanic swarms (Jakobsson et al., 1978). Sample locations are Midfell (Ice-1, 9); Sandfell (Ice-2, 11); Maelifell (Ice-10); Stora-Eldborg (Ice-16); Bleikholl (Ice-25). Base map from Googel Earth ® 2015.

Table 1: Samples, rock type, sample locations, and elevation. Approximate elevations were determined using Lat/Lon and Google Earth ® 2015.

Sample No.	Rock Type	Lat/Lon	Locality	Volcanic System	Elevation (m)
Ice-1[a]	Picrite	64.176N/21.057W	Miðfell	Hengíll	≈ 107
Ice-2[a]	Picrite	64.110N/21.199W	Sandfell	Hengíll	≈ 172
Ice-9[b]	Picrite	64.183N/21.067W	Miðfell	Hengíll	300
Ice-10[a]	Picrite	64.104N/21.202W	Mælifell	Hengíll	344
Ice-11	Picrite	64.110N/21.199W	Sandfell	Hengíll	244
Ice-16[a]	Ol. Thol.	63.857N/22.005W	Stóra-Eldborg	Krýsuvík	100
Ice-25[a]	Ol. Thol.	63.863N/22.356W	Bleikholl	Grindavík	160

[a] Samples from Dixon (2003)

[b] Samples from Dixon et al. (2000)

Table 2: Noble gas data for samples used in this study. All noble gas data are from Dixon et al. (2000) and Dixon (2003).

Sample No.	^{4}He cm^{3} STP/g (1 x 10^{-10})	R/R$_a$	^{20}Ne/^{22}Ne	^{21}Ne/^{22}Ne
Ice-1a[a]	29 ± 2	18 ± 2	10.16 ± 0.11	0.0289 ± 0.0007
Ice-1b[a]	50 ± 3	21 ± 2	10.47 ± 0.07	0.0320 ± 0.0007
Ice-2a[a]	7.0 ± 0.4	14 ± 2	10.07 ± 0.07	0.0306 ± 0.0004
Ice-2b[a]	25 ± 1	11 ± 2	10.50 ± 0.10	0.0335 ± 0.0008
Ice-9a[b]	85 ± 4	20 ± 2	13.3 ± 1.1	0.0308 ± 0.0007
Ice-9b[b]	93 ± 5	29 ± 3	11.98 ± 0.56	0.032 ± 0.002
Ice-9c[b]	79 ± 4	17 ± 1	b.c.	b.c.
Ice-10[a]	58 ± 3	16 ± 1	9.88 ± 0.10	0.0294 ± 0.0005
Ice-11[a]	69 ± 4	17 ± 1	10.1 ± 0.012	0.0301 ± 0.0005
Ice-16[a]	123 ± 7	18 ± 2	10.39 ± 0.09	0.0321 ± 0.0004
Ice-25[a]	112 ± 7	16 ± 1	9.97 ± 0.11	0.0312 ± 0.0004

[a] Samples from Dixon (2003)

[b] Samples from Dixon et al. (2000)

b.c. is "below cut off level" see Dixon et al. (2000) for discussion

3. SAMPLE PREPARATION AND ANALYTICAL METHODS

A total of 107 euhedral to subhedral olivine phenocrysts, ranging in size from ~0.5 to 3 mm, were selected from eight picrite and olivine tholeiite samples. Dixon et al. (2000) and Dixon (2003) were the first to separate the olivine grains used in this study from their host rocks. My volatile study purposely focused on grain populations previously analyzed for their He and Ne isotopic compositions in order to compare the two data sets.

Prior to selection of the olivine grains for volatile analysis, each phenocryst was inspected under a binocular microscope to identify primary melt inclusions trapped during olivine crystallization and to discriminate against melt inclusions showing signs of internal fractures and alteration, thereby reducing the probability of post-entrapment volatile mobility and even diffusion during homogenization. For this study, 157 melt inclusions were homogenized in the Piston Cylinder Laboratory at Rensselaer Polytechnic Institute, following the method outlined in Stefano et al. (2012) and Cabato et al. (2015). Approximately 10–20 olivine grains were packed in dry graphite powder inside a graphite capsule and equilibrated inside the piston cylinder apparatus using a carbon furnace surrounded by a silica glass sleeve and NaCl pressure medium. The charge was heated at 100 ^{o}C/minute for 13 minutes, at 6 kbar pressure, allowed to equilibrate at 1300 ^{o}C for 7 minutes, and was rapidly quenched. As noted by Stefano et al. (2012), to ensure homogenization of melt inclusions (Figure 2), a temperature of 1300 ^{o}C was used to heat the inclusions above the basalt liquidus of approximately 1100-1200 ^{o}C depending on melt composition and water content (e.g., Ghiorso and Sack 1995; Asimow et al., 2001). The high-pressure and temperature homogenization experiments employed here were modeled after Bucholz

et al. (2013). Their procedure showed that melt inclusions with greater than ~0.2 wt. % H_2O are dehydrated to varying degrees during the homogenization experiments. Accordingly, the melt inclusion H_2O concentrations reported here constitute minimum values.

Following homogenization, olivine grains were mounted in an epoxy resin, ground to expose individual melt inclusions, removed, and then polished to 1 μm in a second epoxy mount. The grains were then transferred to an indium mount and polished to 0.3 μm, dried in a vacuum oven at 110 ºC for ~12 hours, gold coated and stored under vacuum prior to analysis. Volatile (H_2O, CO_2, S, F, and Cl) analyses for melt inclusions were conducted at Woods Hole Oceanographic Institution on the Cameca 1280 Secondary Ionization Mass Spectrometer (SIMS) using a primary $^{133}Cs^+$ beam, with a current of 500 nA, rasterized over a 20 x 20 μm area and used to produce the detected secondary ions (^{12}C, $^{16}O^1H$, ^{19}F, ^{30}Si, ^{32}S, and ^{35}Cl). For a detailed description of the analytical and principal method, see Helo et al. (2011) and Hauri et al. (2002), respectively. Calibration curves were produced using a subset of nine standard glasses (Alvin 519-4-1, D51-3, D52-5, 6001, 1654-3, JD17H, D20-3, NS-1, 46D) such that, each element or compound analyzed used a minimum of five standards; seven standards were used to calibrate H_2O. Standard error on the slope of the calibration curve for H_2O was 1.8% or less. The standard errors of the calibration curves were ≤ 9.0%, 8.3%, 3.6% and 11.8 %, for C, F, S, and Cl, respectively. The 1σ stability of the $^{16}O^1H/^{30}Si$ signal for all analyses reported here was 7.4% or better. The 1σ reproducibility of the in-run standard glass Alvin 519-4-1 was 8.2% or better for C, F, S, and Cl and 12.6% for H_2O. For each volatile the secondary ion image was monitored during SIMS analyses (cf. Helo et al., 2011) and volatile data were not included in the discussion if a homogenous signal distribution was not confirmed. Consequently, a total of 21 analyses for C,

three analyses for S, and two analyses for Cl, were not included in the interpretations presented in this study however, all data are reported in the results section.

Following volatile analysis, melt inclusions and host-olivine major-oxide concentrations were measured on the JEOL-JXA-8200 Superprobe at the Massachusetts Institute of Technology Electron Microprobe Facility. Melt inclusions were analyzed with a 15 kv accelerating voltage, a 4 na beam current, and a 10 µm defocused beam size. Typical counting times were 40 s except for Na, which used a sub-counting routine to monitor for beam damage. The standard Alvin 1690-20 was measured 10 times prior to measuring the unknowns and the relative precision for SiO_2, Al_2O_3, FeO, MgO and K_2O were 0.75, 1.40, 0.87, 0.79 and 4.12%, respectively. Host-olivine grains were analyzed using the same setup as the melt inclusions, except that the beam size was only ~1µm.

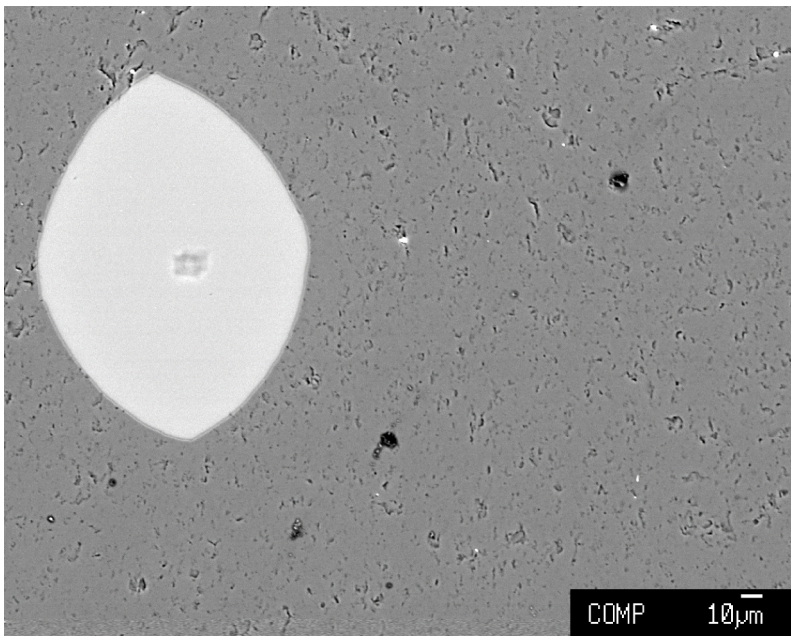

***Figure 2**:* Scanning Electron Microscope (SEM) image of a homogenized and polished olivine-hosted melt inclusion. Ten µm electron microprobe spot in center of melt inclusion.

4. RESULTS

4.1 Olivine Composition

Table 3 summarizes the host-olivine compositions, which, it turns out, are Fo-rich with small variations among sample locations. Host olivine grains in the Hengíll swarm picrite lavas ranged from Fo_{82-92} (Sandfell) to Fo_{85-91} (Miðfell) to Fo_{84-89} (Mælifell). Host-olivine compositions in the olivine tholeiite from Stora-Eldborg in the Krýsuvík volcanic system have a narrow range of Fo_{83-84}. The olivine tholeiite from Bleikholl in the Grindavík swarm, *Ice-25*, shows a range of Fo_{83-87}.

Table 3. Host-olivine Compositions.

Sample	SiO_2	TiO_2	Al_2O_3	FeO	MnO	MgO	CaO	NiO	Total	Fo (mol %)
Ice-1.1	40.64	0.00	0.05	10.18	0.11	49.05	0.36	0.26	100.6	89.6
Ice-1.2	40.53	0.00	0.07	9.02	0.10	49.99	0.32	0.31	100.3	90.8
Ice-1.3	40.05	0.02	0.15	13.60	0.19	46.47	0.32	0.17	101.0	85.9
Ice-1.4	39.92	0.00	0.08	12.19	0.18	47.50	0.36	0.20	100.4	87.4
Ice-1.5	40.54	0.01	0.15	11.27	0.13	48.18	0.32	0.19	100.8	88.4
Ice-1.7	40.22	0.03	0.08	11.16	0.18	48.36	0.30	0.21	100.5	88.5
Ice-1.8	39.64	0.04	0.06	12.50	0.23	47.41	0.32	0.20	100.4	87.1
Ice-1.9	39.42	0.02	0.13	9.68	0.17	49.35	0.31	0.23	99.3	90.1
Ice-1.10	40.20	0.04	0.06	9.64	0.15	49.56	0.32	0.24	100.2	90.2
Ice-1.11	40.55	0.01	0.07	10.02	0.16	48.87	0.32	0.24	100.2	89.7
Ice-1.12	39.73	0.01	0.10	11.05	0.17	48.34	0.33	0.23	100.0	88.6
Ice-1.13	40.14	0.03	0.05	8.59	0.13	50.39	0.31	0.27	99.9	91.3
Ice-1.14	39.56	0.01	0.05	12.60	0.20	47.39	0.28	0.18	100.3	87.0
Ice-1.15	40.20	0.03	0.06	12.15	0.21	47.46	0.33	0.19	100.6	87.4
Ice-1.16	39.80	0.02	0.06	11.36	0.16	48.03	0.32	0.20	99.9	88.3
Ice-2.1	39.01	0.00	0.02	12.91	0.22	47.45	0.32	0.16	100.1	86.8
Ice-2.2	40.36	0.01	0.14	10.90	0.17	48.17	0.27	0.27	100.3	88.7
Ice-2.3	39.04	0.00	0.01	12.13	0.24	47.80	0.31	0.19	99.7	87.5
Ice-2.4	38.88	0.00	0.00	10.48	0.19	49.43	0.30	0.24	99.5	89.4
Ice-2.5	38.96	0.00	0.06	17.39	0.30	43.36	0.32	0.14	100.5	81.6
Ice-2.6	40.13	0.00	0.11	10.38	0.18	49.26	0.27	0.26	100.6	89.4
Ice-2.7	39.56	0.00	0.00	10.57	0.18	49.05	0.33	0.22	99.9	89.2

Table 3. (Continued). Host-olivine Compositions.

Sample	SiO_2	TiO_2	Al_2O_3	FeO	MnO	MgO	CaO	NiO	Total	Fo (mol %)
Ice-2.8	40.19	0.00	0.07	10.91	0.20	47.76	0.31	0.22	99.7	88.6
Ice-2.9	40.60	0.00	0.04	12.32	0.19	47.13	0.34	0.21	100.8	87.2
Ice-2.10	39.41	0.00	0.07	10.98	0.16	48.84	0.31	0.22	100.0	88.8
Ice-2.11	39.54	0.00	0.07	9.45	0.14	49.29	0.30	0.28	99.1	90.3
Ice-2.12	40.07	0.00	0.07	10.03	0.17	49.69	0.35	0.24	100.6	89.8
Ice-2.13	40.19	0.00	0.05	12.78	0.22	46.90	0.31	0.17	100.6	86.7
Ice-2.14	39.51	0.00	0.03	12.23	0.20	47.55	0.32	0.20	100.0	87.4
Ice-2.15	40.22	0.00	0.81	12.57	0.22	46.70	0.34	0.19	101.0	86.9
Ice-2.16	40.24	0.00	0.09	10.42	0.17	49.24	0.30	0.28	100.7	89.4
Ice-9.1	40.24	0.00	0.03	11.55	0.16	47.65	0.33	0.16	100.1	88.0
Ice-9.2	40.15	0.00	0.03	11.02	0.16	48.04	0.32	0.20	99.9	88.6
Ice-9.3	39.25	0.00	0.89	12.76	0.22	45.79	0.37	0.16	99.4	86.5
Ice-9.4	40.11	0.00	0.01	9.76	0.14	49.10	0.34	0.24	99.7	90.0
Ice-9.5	39.53	0.00	0.02	10.75	0.16	48.45	0.33	0.23	99.5	88.9
Ice-9.6	40.40	0.00	0.10	9.51	0.15	49.52	0.33	0.24	100.3	90.3
Ice-9.7	40.14	0.00	0.11	11.52	0.17	47.89	0.37	0.21	100.4	88.1
Ice-9.8	39.90	0.00	0.08	11.16	0.19	48.55	0.32	0.19	100.4	88.6
Ice-9.9	40.21	0.00	0.02	11.01	0.18	48.49	0.32	0.24	100.5	88.7
Ice-9.10	39.35	0.00	0.02	10.94	0.17	48.56	0.35	0.22	99.6	88.8
Ice-9.11	40.35	0.00	0.04	10.22	0.16	49.10	0.34	0.24	100.5	89.5
Ice-9.12	39.55	0.00	0.01	9.65	0.17	49.78	0.31	0.27	99.7	90.2
Ice-9.13	40.52	0.00	0.03	9.97	0.15	49.56	0.32	0.23	100.8	89.9
Ice-9.14	40.00	0.00	0.04	14.07	0.23	46.49	0.34	0.16	101.3	85.5
Ice-10.1	39.24	0.00	0.04	10.36	0.18	49.06	0.31	0.23	99.4	89.4
Ice-10.2	39.71	0.00	0.15	12.45	0.21	47.44	0.30	0.16	100.4	87.2
Ice-10.3	40.08	0.00	0.06	12.77	0.18	47.71	0.32	0.16	101.3	86.9
Ice-10.4	39.76	0.04	0.07	12.47	0.18	47.55	0.33	0.16	100.6	87.2
Ice-10.5	39.58	0.01	0.05	12.11	0.20	48.08	0.33	0.14	100.5	87.6
Ice-10.6	40.05	0.01	0.03	12.54	0.20	47.64	0.32	0.21	101.0	87.1
Ice-10.7	39.59	0.06	0.02	12.88	0.21	46.97	0.31	0.17	100.2	86.7
Ice-10.8	39.07	0.00	0.07	9.65	0.13	49.42	0.28	0.24	98.9	90.1
Ice-10.9	39.91	0.00	0.06	9.51	0.13	49.76	0.31	0.28	100.0	90.3
Ice-10.10	39.46	0.03	0.07	12.76	0.19	47.38	0.33	0.16	100.4	86.9
Ice-10.11	38.77	0.04	0.06	15.80	0.27	45.22	0.29	0.12	100.6	83.6
Ice-10.12	39.34	0.01	0.06	13.16	0.20	47.09	0.30	0.16	100.3	86.4
Ice-10.13	40.12	0.00	0.11	13.25	0.19	46.93	0.31	0.14	101.1	86.3
Ice-10.14	40.20	0.00	0.08	12.34	0.17	47.59	0.32	0.18	100.9	87.3
Ice-10.15	40.08	0.00	0.05	12.15	0.13	47.81	0.35	0.16	100.7	87.5
Ice-10.16	40.11	0.00	0.04	11.70	0.15	48.24	0.33	0.16	100.7	88.0
Ice-10.17	39.91	0.00	0.05	12.79	0.20	47.27	0.35	0.16	100.7	86.8
Ice-10.18	39.48	0.00	0.06	11.96	0.21	47.82	0.31	0.18	100.0	87.7
Ice-10.19	39.05	0.00	0.06	12.80	0.22	47.48	0.34	0.19	100.1	86.9
Ice-10.20	39.90	0.03	0.30	11.09	0.22	48.43	0.30	0.23	100.5	88.6
Ice-10.21	39.80	0.00	0.07	12.12	0.22	47.64	0.33	0.18	100.4	87.5
Ice-10.22	39.38	0.00	0.06	12.50	0.20	47.45	0.33	0.19	100.1	87.1
Ice-10.23	39.15	0.00	0.04	12.02	0.20	48.36	0.32	0.18	100.3	87.8
Ice-10.24	39.20	0.00	0.01	12.49	0.21	47.67	0.28	0.16	100.0	87.2
Ice-10.25	39.45	0.00	0.25	14.43	0.26	45.80	0.31	0.14	100.6	85.0
Ice-11.1	40.47	0.07	0.10	10.07	0.18	48.91	0.33	0.38	100.5	89.6
Ice-11.2	39.89	0.07	0.07	11.68	0.22	47.96	0.31	0.27	100.5	88.0
Ice-11.3	40.10	0.06	0.10	11.39	0.18	48.49	0.35	0.24	100.9	88.4
Ice-11.4	39.68	0.08	0.11	12.04	0.21	48.41	0.32	0.24	101.1	87.8

Table 3. (Continued). Host-olivine Compositions.

Sample	SiO_2	TiO_2	Al_2O_3	FeO	MnO	MgO	CaO	NiO	Total	Fo (mol %)
Ice-11.5	40.68	0.04	0.08	8.11	0.15	50.74	0.29	0.35	100.4	91.8
Ice-11.6	37.69	0.03	0.09	9.98	0.18	49.41	0.32	0.33	98.0	89.8
Ice-11.7	40.79	0.04	0.11	9.61	0.17	49.64	0.33	0.32	101.0	90.2
Ice-11.8	40.42	0.07	0.12	9.93	0.19	49.09	0.34	0.32	100.5	89.8
Ice-11.9	40.00	0.04	0.10	12.24	0.22	47.74	0.34	0.26	100.9	87.4
Ice-11.10	40.70	0.02	0.08	8.66	0.15	50.80	0.34	0.35	101.1	91.3
Ice-11.11	40.31	0.04	0.13	10.84	0.22	48.88	0.34	0.24	101.0	88.9
Ice-11.12	40.42	0.05	0.12	11.04	0.22	48.69	0.31	0.28	101.1	88.7
Ice-11.13	40.88	0.02	0.10	9.01	0.20	50.05	0.34	0.30	100.9	90.8
Ice-11.14	40.92	0.05	0.14	10.10	0.20	49.15	0.36	0.31	101.2	89.7
Ice-11.15	40.21	0.05	0.11	11.72	0.23	48.45	0.37	0.26	101.4	88.0
Ice-16.1	39.16	0.06	0.64	16.32	0.33	44.09	0.26	0.23	101.1	82.8
Ice-16.2	39.99	0.06	0.11	15.42	0.29	45.65	0.31	0.25	102.1	84.1
Ice-16.3	39.22	0.07	0.12	15.25	0.26	46.09	0.28	0.23	101.5	84.3
Ice-16.4	39.74	0.11	0.16	16.13	0.27	44.58	0.28	0.24	101.5	83.1
Ice-16.5	39.92	0.08	0.07	15.12	0.23	45.58	0.26	0.24	101.5	84.3
Ice-16.6	39.83	0.06	0.13	15.23	0.27	45.43	0.29	0.24	101.5	84.2
Ice-16.7	39.83	0.07	0.09	15.51	0.30	45.53	0.29	0.26	101.9	83.9
Ice-16.8	39.85	0.14	0.12	15.24	0.23	45.14	0.28	0.22	101.2	84.1
Ice-16.9	39.82	0.07	0.09	15.33	0.23	45.53	0.27	0.27	101.6	84.1
Ice-25.1	39.96	0.00	0.02	13.97	0.21	46.37	0.26	0.23	101.0	85.5
Ice-25.2	39.53	0.01	0.02	15.10	0.24	45.47	0.27	0.19	100.8	84.3
Ice-25.3	39.63	0.00	0.06	14.63	0.21	45.07	0.33	0.17	100.1	84.6
Ice-25.4	39.45	0.00	0.05	14.95	0.24	45.34	0.27	0.21	100.5	84.4
Ice-25.5	39.35	0.00	0.02	14.84	0.23	45.19	0.27	0.17	100.1	84.4
Ice-25.6	40.03	0.00	0.27	14.32	0.21	45.30	0.30	0.17	100.6	84.9
Ice-25.7	39.66	0.00	0.02	14.92	0.21	45.42	0.28	0.16	100.7	84.4
Ice-25.8	39.53	0.04	0.04	15.07	0.24	45.38	0.28	0.15	100.7	84.3
Ice-25.9	39.15	0.01	0.02	16.63	0.25	44.08	0.29	0.12	100.6	82.5
Ice-25.10	38.11	0.00	0.01	14.47	0.25	45.67	0.25	0.20	99.0	84.9
Ice-25.11	38.83	0.05	0.06	14.56	0.23	46.05	0.28	0.19	100.2	84.9
Ice-25.12	39.79	0.00	0.00	14.84	0.25	45.24	0.28	0.18	100.6	84.5
Ice-25.13	40.09	0.00	0.01	12.35	0.18	47.82	0.25	0.23	100.9	87.3

4.2 Major Elements in Melt Inclusions

Measured major-oxide and volatile element concentrations for all melt inclusion analyses are listed in Table 4. The major-oxide concentrations of the Reykjanes Peninsula melt inclusions indicate that the majority are tholeiitic basalts (Figure 3.A and Figure 3.B); with only six melt inclusions classified as belonging to the alkaline series (Figure 3b). Melt inclusions range in Mg# (58-77) with a majority bearing higher Mg# and more primitive composition than the glasses reported for the Hengíll swarm by Tronnes (1990). Melt inclusion major-oxide concentrations can be related to the basaltic-glass data from Tronnes (1990) by the progressive crystallization of olivine and plagioclase, present as phenocrysts in all samples (Figure 4). The major-oxide concentrations in the melt inclusions extend the basaltic glass trends from Tronnes (1990) to less differentiated compositions (Figure 4).

The melt Inclusion data show a broader scatter than the data from Tronnes (1990). FeO^t concentrations for the melt inclusions show a range (7.41-13.32 wt. %); several of these data are in agreement with the basaltic glasses analyzed by Tronnes (1990), which show a range of 8.75-15.13 wt. % but the melt inclusion data reported here exhibit more variability (Figure 4). The variability in FeO^t and MgO in the melt inclusion is often the result of edge effects (Cabato et al., 2015) and interpretations of these data are limited.

Table 4: Major oxide and volatile data for all melt inclusions analyzed in this study. Major oxides and H_2O concentrations are in wt. %. Carbon, F, S, and Cl concentrations are ppm. 2σ uncertainties are shown for volatile data.

Sample	SiO_2	TiO_2	Al_2O_3	Cr_2O_3	FeO	MnO	MgO	CaO	Na_2O	K_2O	SO_3	Total	H_2O (wt%)	C (ppm)	F (ppm)	S (ppm)	Cl (ppm)
Ice-1.1	47.07	1.03	13.77	0.09	8.94	0.16	14.25	12.64	1.39	0.18	0.14	99.7	0.11 ± 0.003	564 ± 53	42.7 ± 0.79	906 ± 28	77.8 ± 8.0
Ice-1.2	48.63	0.59	14.25	0.3	7.52	0.12	13.89	12.78	1.81	0.04	0.07	100.0	0.36 ± 0.008	36.6 ± 4.2	74.2 ± 1.6	683 ± 46	21.2 ± 2.2
Ice-1.3a	48.51	0.86	15.34	0.04	10.93	0.2	8.88	14.04	1.4	0.06	0.07	100.3	0.28 ± 0.006	51.6 ± 6.4	61.9 ± 1.5	539 ± 17	11.9 ± 1.2
Ice-1.3b	47.02	0.76	13.42	0.02	10.96	0.21	13.09	12.68	1.31	0.03	0.1	99.6	0.20 ± 0.004	46.7 ± 4.9	57.2 ± 1.1	556 ± 17	7.48 ± 0.77
Ice-1.3c	48.28	0.79	15.23	0.01	9.64	0.15	13.5	11.88	1.69	0.04	0.06	101.3	0.19 ± 0.004	40.1 ± 6.4	74.5 ± 1.5	534 ± 17	53.7 ± 5.5
Ice-1.3d	47.37	0.74	15.02	0.06	10.85	0.17	12.75	11.05	1.96	0.07	0.11	100.2	0.24 ± 0.005	2660 ± 1600	141 ± 2.9	696 ± 34	107 ± 11
Ice-1.4	47.51	1.87	14.59	0.08	10.95	0.21	9.06	14.48	1.2	0.13	0.14	100.2	0.58 ± 0.01	321 ± 30	66.5 ± 1.4	899 ± 29	84.6 ± 8.7
Ice-1.5	47.38	0.81	14.69	0.06	9.72	0.17	11.34	13.08	1.47	0.03	0.06	98.8	0.51 ± 0.01	65.6 ± 7.4	59.7 ± 1.1	357 ± 11	32.1 ± 3.3
Ice-1.6	47.11	0.63	14.17	0.46	8.68	0.17	13.02	13.61	1.26	0.04	0.07	99.2	0.35 ± 0.007	157 ± 15	38.2 ± 0.74	415 ± 13	6.66 ± 0.69
Ice-1.7	47.27	1.05	14.35	0.14	9.99	0.21	12.92	11.79	1.74	0.16	0.11	99.7	0.30 ± 0.006	471 ± 650	72.0 ± 1.3	806 ± 26	91.8 ± 9.5
Ice-1.8	48.95	1.08	15.96	0.05	9.86	0.17	8.8	13.68	1.65	0.22	0.14	100.6	0.33 ± 0.007	73.0 ± 8.8	71.8 ± 1.4	738 ± 23	88.5 ± 9.1
Ice-1.9a	48.18	0.59	14.71	0.29	8.22	0.13	13.01	13.56	1.56	0.03	0.06	100.3	0.30 ± 0.009	46.7 ± 4.6	34.9 ± 1.1	451 ± 15	1.82 ± 0.19
Ice-1.9b	48.68	0.66	16.74	0.14	7.6	0.12	11	13.92	1.58	0.02	0.08	100.5	0.50 ± 0.02	0.185 ± 13	37.7 ± 1.3	424 ± 15	1.45 ± 0.17
Ice-1.9c	48.63	0.63	15.36	0.15	8.11	0.12	10.89	14.32	1.52	0.01	0.04	99.8	0.43 ± 0.009	72.0 ± 6.9	39.9 ± 0.81	417 ± 13	1.44 ± 0.17
Ice-1.9d	47.18	0.66	14.48	0.29	8.57	0.14	13.63	13.19	1.74	0.03	0.05	100.0	0.17 ± 0.003	292 ± 27	41.3 ± 0.76	477 ± 15	19.5 ± 2.0
Ice-1.10a	47.53	0.71	14.24	0.17	8.39	0.11	13.85	13.13	1.4	0.27	0.08	99.9	0.34 ± 0.007	32.7 ± 4.0	44.1 ± 0.86	918 ± 190	112 ± 12
Ice-1.10b	48.38	0.53	15.19	0.39	8.1	0.13	11.25	13.88	1.34	0.09	0.06	99.3	0.43 ± 0.008	195 ± 18	38.8 ± 0.73	341 ± 11	31.6 ± 3.2
Ice-1.10c	49.24	0.68	16.53	0.34	7.45	0.1	9.14	14.26	1.7	0.17	0.07	99.7	0.39 ± 0.008	121 ± 12	39.8 ± 0.77	552 ± 17	63.1 ± 6.5
Ice-1.11	47.88	0.65	14.64	0.12	8.45	0.13	13.07	13.21	1.49	0.02	0.08	99.7	0.21 ± 0.004	300 ± 28	36.5 ± 0.77	497 ± 16	3.67 ± 0.38
Ice-1.12	48.25	0.5	15.46	0.74	9.06	0.12	10.48	13.22	1.58	0.01	0.11	99.5	0.61 ± 0.01	48.6 ± 5.2	59.0 ± 1.1	510 ± 17	1.40 ± 0.15
Ice-1.13a	49.77	0.58	16.57	0.2	6.8	0.12	10.19	14.39	1.61	0	0	100.2	0.41 ± 0.01	28.9 ± 6.1	60.7 ± 1.7	15.1 ± 0.56	1.31 ± 0.20
Ice-1.13b	50.65	0.63	18.45	0.14	6.12	0.09	8.58	14.46	1.98	0.01	0	101.1	0.51 ± 0.01	20.1 ± 4.2	63.5 ± 1.2	4.97 ± 0.20	1.00 ± 0.11
Ice-1.14a	46.89	0.47	14.19	0.08	11.27	0.19	11.57	14.57	0.92	0.02	0.07	100.2	0.19 ± 0.004	294 ± 28	75.2 ± 1.5	602 ± 19	12.7 ± 1.3
Ice-1.	47.7	0.51	13.89	0.06	10.81	0.22	12.7	13.18	1.26	0.03	0.07	100.4	0.28 ± 0.005	580 ± 53	67.6 ± 1.3	576 ± 18	7.58 ± 0.78
Ice-1.14c	47.59	0.47	13.62	0.04	10.66	0.18	13.9	12.77	1.27	0.01	0.09	100.6	0.21 ± 0.004	205 ± 19	70.1 ± 1.3	591 ± 19	12.7 ± 1.3
Ice-1.15	47.47	0.89	13.97	0.07	10.42	0.19	13.49	11.44	1.77	0.18	0.13	100.0	0.31 ± 0.006	2150 ± 2800	79.9 ± 1.5	1040 ± 79	104 ± 11
Ice-1.16a	48.22	0.65	15.04	0.08	10	0.17	13.99	11.43	1.28	0.07	0.06	101.0	0.44 ± 0.009	53.6 ± 6.2	76.6 ± 1.4	674 ± 21	70.4 ± 7.3
Ice-1.16b	47.93	0.48	14.16	0.08	9.51	0.17	13.12	13.06	1.16	0.03	0.08	99.8	0.24 ± 0.005	707 ± 65	47.1 ± 0.90	637 ± 21	8.91 ± 0.95
Ice-1.16c	48.44	0.3	13.87	0.07	9.42	0.19	13.83	12.94	1.08	0.02	0.1	100.3	0.23 ± 0.004	641 ± 58	45.1 ± 0.86	665 ± 21	3.85 ± 0.41
Ice-1.16d	47.87	0.71	14.72	0.33	10.14	0.16	14.27	10.96	1	0.05	0.09	100.3	0.34 ± 0.007	1310 ± 120	45.7 ± 0.94	540 ± 17	33.1 ± 3.4
Ice-2.1	47.91	1.57	14.73	0.04	10.09	0.18	9.68	13.41	1.34	0.19	0.11	99.3	0.62 ± 0.01	1290 ± 190	67.0 ± 2.0	661 ± 21	97.4 ± 10
Ice-2.2a	48.68	0.44	15.12	0.57	9.63	0.17	10.62	12.6	1.76	0.01	0.07	99.7	0.57 ± 0.01	106 ± 32	56.8 ± 1.5	433 ± 23	2.71 ± 0.29
Ice-2.2b	47.8	0.66	15.39	0.06	8.78	0.15	13	12.51	1.72	0.05	0.09	100.2	0.47 ± 0.01	696 ± 360	52.8 ± 1.2	460 ± 15	13.6 ± 1.4
Ice-2.3	46.18	0.57	15.8	0.52	10.01	0.16	12.22	13.06	1.59	0.06	0.02	100.2	0.36 ± 0.007	20.5 ± 2.3	54.3 ± 1.1	38.9 ± 1.3	4.59 ± 0.48

Table 4: (Continued). Major oxide and volatile data for all melt inclusions analyzed in this study. Major oxides and H_2O concentrations are in wt. %. Carbon, F, S, and Cl concentrations are ppm. 2σ uncertainties are shown for volatile data.

Sample	SiO_2	TiO_2	Al_2O_3	Cr_2O_3	FeO	MnO	MgO	CaO	Na_2O	K_2O	SO_3	Total	H_2O (wt%)	C (ppm)	F (ppm)	S (ppm)	Cl (ppm)
Ice-2.4	48.74	1.61	16.56	0.12	8.1	0.12	9.24	13.66	1.72	0.26	0.1	100.2	0.28 ± 0.006	270 ± 30	74.9 ± 1.5	757 ± 24	80.4 ± 8.2
Ice-2.5a	47.37	0.7	13.77	0.08	10.76	0.15	12.98	11.98	1.74	0.05	0.06	99.6	0.61 ± 0.01	506 ± 870	75.0 ± 1.4	268 ± 9.1	18.5 ± 1.9
Ice-2.5b	46.36	0.14	19.06	0.1	10.71	0.22	10.91	11.69	1.22	0.05	0.04	100.5	0.33 ± 0.006	16.6 ± 3.5	17.3 ± 0.36	17.0 ± 0.56	1.64 ± 0.18
Ice-2.6	45.5	0.92	15.54	0.5	12.52	0.15	13.03	9.4	2.05	0.07	0.22	99.9	0.70 ± 0.02	63.4 ± 7.5	91.4 ± 2.3	1320 ± 43	74.8 ± 7.8
Ice-2.7	48.24	1.18	14.31	0.12	8.8	0.16	12.85	12.63	1.5	0.16	0.15	100.1	0.20 ± 0.004	414 ± 38	57.7 ± 1.2	934 ± 36	54.9 ± 5.6
Ice-2.8	47.51	1.82	15.41	0.09	9.12	0.16	10.19	13.91	1.28	0.1	0.03	99.6	0.51 ± 0.01	29.1 ± 4.3	73.0 ± 1.5	209 ± 6.8	21.3 ± 2.2
Ice-2.9a	45.97	1.01	13.67	0.05	10.96	0.19	12.84	13.36	1.3	0.04	0.06	99.5	0.86 ± 0.02	126 ± 1700	79.6 ± 1.6	428 ± 13	54.8 ± 5.6
Ice-2.9b	48.08	0.71	13.95	0.04	9.58	0.17	13.28	12.63	1.51	0.05	0.08	100.1	0.62 ± 0.01	648 ± 120	62.0 ± 1.2	370 ± 12	14.2 ± 1.5
Ice-2.9c	42.82	1.58	15.51	0.09	13.88	0.22	7.92	12.6	2.34	0.07	0.08	97.1	1.99 ± 0.06	648 ± 62	110 ± 2.4	518 ± 20	74.5 ± 7.7
Ice-2.10a	48	1.04	14.78	0.08	8.77	0.18	10.06	14.68	1.65	0.12	0.06	99.4	0.47 ± 0.009	420 ± 45	63.5 ± 1.3	561 ± 18	49.4 ± 5.1
Ice-2.10b	47.31	1.15	13.75	0.08	9.53	0.15	11.28	13.98	1.35	0.19	0.09	98.9	0.49 ± 0.01	325 ± 29	62.4 ± 1.2	664 ± 21	82.9 ± 8.6
Ice-2.11	48.89	0.61	15.25	0.26	7.41	0.12	12.06	13.63	1.78	0.02	0.05	100.1	0.38 ± 0.008	16.9 ± 2.5	63.1 ± 1.3	323 ± 10	1.11 ± 0.12
Ice-2.12	47.14	0.67	15.31	0.37	8.78	0.15	13.15	12.57	1.54	0.03	0.06	99.8	0.56 ± 0.01	113 ± 12	55.0 ± 1.3	340 ± 11	18.2 ± 1.9
Ice-2.13	44.46	1.33	14.06	0.06	12.62	0.2	10.88	14.79	1.29	0.08	0.12	99.9	0.80 ± 0.02	251 ± 26	65.7 ± 1.3	1060 ± 93	52.8 ± 5.4
Ice-2.14	48.28	0.9	13.88	0.05	10.02	0.18	11.74	12.72	1.51	0.09	0.13	99.5	0.90 ± 0.02	93.8 ± 8.8	76.1 ± 2.2	729 ± 23	26.8 ± 2.8
Ice-2.15	48.62	0.83	14.26	0.04	9.94	0.17	14.05	12.21	1.58	0.11	0.14	102.0	0.81 ± 0.03	115 ± 13	86.4 ± 10	950 ± 62	29.8 ± 3.6
Ice-2.16	49.8	0.51	15.94	0.77	8.8	0.16	8.16	13.53	2.27	0.01	0.1	100.1	0.54 ± 0.01	53.5 ± 7.2	66.4 ± 1.2	526 ± 17	1.73 ± 0.19
Ice-9.1	48.61	0.6	14.31	0.1	9.28	0.15	12.22	13.21	1.36	0.11	0.08	100.0	0.49 ± 0.01	31.6 ± 2.3	68.3 ± 5.7	401 ± 13	25.5 ± 3.0
Ice-9.2	48.22	0.88	15.13	0.11	8.99	0.15	10.34	13.3	1.58	0.12	0.14	99.0	0.46 ± 0.01	42.7 ± 17	46.9 ± 3.9	582 ± 20	47.3 ± 5.6
Ice-9.3	47.91	0.85	14.81	0.03	10.4	0.18	10.88	13.24	1.49	0.02	0.13	99.9	0.67 ± 0.01	146 ± 4.8	60.3 ± 5.0	540 ± 18	10.5 ± 1.3
Ice-9.4	46.62	0.73	14.24	0.53	8.04	0.13	12.23	12.99	1.1	0.21	0.09	96.9	0.78 ± 0.02	99.5 ± 18	49.3 ± 4.1	427 ± 14	101 ± 12
Ice-9.5	46.97	0.81	13.84	0.15	9.87	0.19	12.47	13.94	1.35	0.01	0.1	99.7	0.54 ± 0.01	215 ± 52	45.3 ± 0.89	384 ± 12	3.85 ± 0.41
Ice-9.6a	47.6	0.78	16.09	0.37	7.98	0.16	9.72	14.53	1.38	0.01	0.11	98.7	0.50 ± 0.01	178 ± 17	42.9 ± 0.85	387 ± 12	2.28 ± 0.25
Ice-9.6b	47.71	0.81	15.9	0.15	8	0.16	10.98	14.13	1.47	0.01	0.1	99.4	0.39 ± 0.008	145 ± 15	39.7 ± 0.77	441 ± 14	2.29 ± 0.25
Ice-9.6c	46.03	1.07	16.25	0.34	7.63	0.14	8.38	13.85	1.44	0.01	0.11	95.3	0.43 ± 0.009	215 ± 21	39.4 ± 0.86	411 ± 13	2.38 ± 0.25
Ice-9.7	46.94	0.81	16.42	0.13	9.22	0.14	10.34	13.08	1.58	0.02	0.13	98.8	0.46 ± 0.009	33.0 ± 5.2	68.2 ± 1.3	487 ± 16	3.45 ± 0.37
Ice-9.8a	47.13	0.73	14.8	0.6	8.99	0.14	11.84	12.2	1.56	0.06	0.04	98.1	0.31 ± 0.006	54.0 ± 6.0	54.8 ± 1.2	98.5 ± 3.3	10.1 ± 1.1
Ice-9.8b	47.97	0.62	15.08	0.72	9.38	0.18	11.64	12.68	1.51	0.03	0.02	99.8	0.34 ± 0.008	30.6 ± 4.3	61.8 ± 1.2	34.6 ± 1.1	3.74 ± 0.40
Ice-9.8c	48.51	0.77	15.72	0.12	8.91	0.16	9.65	13.55	1.6	0.15	0.12	99.3	0.52 ± 0.01	73.3 ± 7.7	61.1 ± 1.2	531 ± 17	72.8 ± 7.5
Ice-9.9a	47.34	0.68	14.87	0.44	9.15	0.16	12.5	12.31	1.49	0.25	0.18	99.4	0.28 ± 0.006	321 ± 30	53.2 ± 0.98	756 ± 25	101 ± 10
Ice-9.9b	48.99	0.72	16.81	0.11	8.85	0.17	7.63	14.38	1.78	0.07	0.05	99.6	0.41 ± 0.04	181 ± 23	57.4 ± 2.0	538 ± 18	51.8 ± 5.7
Ice-9.10	48.01	0.81	15.27	0.1	8.91	0.14	12.74	13.13	1.72	0.04	0.03	100.9	0.30 ± 0.006	35.0 ± 4.9	50.5 ± 1.0	78.9 ± 2.5	6.38 ± 0.66
Ice-9.11	47.91	0.59	15.07	0.26	8.51	0.14	12.81	13.49	1.3	0	0.09	100.2	0.26 ± 0.005	69.3 ± 7.8	34.5 ± 0.65	387 ± 12	1.26 ± 0.15
Ice-9.12	49.04	0.62	15.63	0.17	7.93	0.15	11.37	14.04	1.23	0.01	0.08	100.3	0.54 ± 0.01	70.0 ± 7.0	41.2 ± 0.82	271 ± 8.5	0.975 ± 0.11
Ice-9.13	49.09	0.78	15.58	0.14	8.17	0.14	10.56	14.6	1.44	0.09	0.14	100.7	0.30 ± 0.006	227 ± 21	50.1 ± 1.2	529 ± 17	34.8 ± 3.6
Ice-9.14	47.75	1.53	13.95	0.05	12.05	0.23	10.57	12.5	1.48	0.13	0.18	100.4	0.48 ± 0.009	51.2 ± 5.7	59.3 ± 1.1	791 ± 25	61.7 ± 6.3
Ice-9.15a	50.11	0.46	10.27	0.63	7.67	0.12	12.64	17.19	1.11	0.02	0.06	100.3	0.30 ± 0.006	3510 ± 360	45.0 ± 1.0	294 ± 9.7	8.22 ± 0.92
Ice-9.15b	49.67	0.67	9.79	0.61	7.52	0.15	12.84	17.39	0.87	0.02	0.04	99.6	0.32 ± 0.007	714 ± 65	42.0 ± 0.81	221 ± 7.2	4.96 ± 0.52

Table 4: (Continued). Major oxide and volatile data for all melt inclusions analyzed in this study. Major oxides and H_2O concentrations are in wt. %. Carbon, F, S, and Cl concentrations are ppm. 2σ uncertainties are shown for volatile data.

Sample	SiO_2	TiO_2	Al_2O_3	Cr_2O_3	FeO	MnO	MgO	CaO	Na_2O	K_2O	SO_3	Total	H_2O (wt%)	C (ppm)	F (ppm)	S (ppm)	Cl (ppm)
Ice-9.16	49.99	0.64	9.9	0.55	8.24	0.16	12.59	16.86	1.1	0	0.07	100.1	0.33 ± 0.007	9620 ± 3500	43.5 ± 0.83	298 ± 9.7	17.9 ± 2.6
Ice-10.1	48.84	0.56	15.34	0.81	8.43	0.14	10.63	13.58	1.66	0	0	100.0	0.77 ± 0.02	78.4 ± 7.4	71.4 ± 2.8	375 ± 12	30.6 ± 3.3
Ice-10.2	46.44	0.91	14.23	0.09	10.55	0.17	12.86	12.71	1.54	0.19	0.17	99.9	0.37 ± 0.007	36.2 ± 5.3	59.9 ± 1.2	944 ± 30	91.2 ± 9.4
Ice-10.3	46.38	1.03	13.31	0.1	10.53	0.16	13.93	12.85	1.41	0.12	0.13	100.0	0.55 ± 0.01	2010 ± 4200	72.4 ± 1.4	1200 ± 39	61.5 ± 6.3
Ice-10.4	47.16	0.9	13.69	0.09	10.08	0.17	12.98	12.51	1.34	0.2	0.28	99.4	0.43 ± 0.008	22000 ± 37000	63.1 ± 1.2	2800 ± 1200	102 ± 10
Ice-10.5a	41.07	0.66	13.32	0.21	9.67	0.15	12.7	12.02	1.39	0.12	0.15	91.5	0.30 ± 0.007	144 ± 16	66.6 ± 1.4	716 ± 24	67.6 ± 7.0
Ice-10.5b	48.24	0.87	13.82	0.14	9.53	0.13	14.34	11.81	1.54	0.15	0.18	100.8	0.30 ± 0.007	142 ± 13	72.8 ± 1.6	743 ± 24	66.0 ± 6.8
Ice-10.5c	48.23	0.84	13.42	0.09	9.48	0.14	13.1	12.58	1.36	0.12	0.14	99.5	0.45 ± 0.009	38.7 ± 8.9	83.6 ± 1.5	632 ± 20	59.7 ± 6.1
Ice-10.6	48.16	1.28	13.91	0.1	9.9	0.18	12.45	11.93	1.66	0.22	0.11	99.9	0.46 ± 0.01	27.6 ± 3.3	62.1 ± 1.3	783 ± 25	103 ± 11
Ice-10.7a	46.73	1.44	13.58	0.06	10.67	0.19	13.06	11.3	1.79	0.29	0.27	99.4	0.30 ± 0.006	401 ± 43	68.8 ± 1.3	1120 ± 57	138 ± 14
Ice-10.7b	47.33	1.56	13.14	0.12	10.92	0.18	12.92	11.52	1.73	0.25	0.3	100.0	0.33 ± 0.007	352 ± 33	71.6 ± 1.4	1040 ± 36	123 ± 13
Ice-10.7c	47.51	2.05	13.58	0.09	10.11	0.17	7.72	13.72	1.85	0.19	0.21	97.2	0.93 ± 0.02	276 ± 26	82.4 ± 1.6	903 ± 28	96.6 ± 9.9
Ice-10.8a	47.32	0.68	14.33	0.47	8.44	0.14	12.57	13.59	1.55	0	0	99.1	0.79 ± 0.02	201 ± 200	61.9 ± 1.3	344 ± 14	16.4 ± 1.7
Ice-10.8b	46.85	0.71	14.55	0.77	8.44	0.11	12.37	13.58	1.53	0	0.03	98.9	0.71 ± 0.01	2660 ± 1200	61.2 ± 1.2	339 ± 11	10.6 ± 1.5
Ice-10.9	47.51	0.49	14.58	0.66	7.96	0.1	14.29	12.64	1.61	0	0.02	99.9	0.43 ± 0.008	59.9 ± 6.1	55.4 ± 1.0	514 ± 17	5.56 ± 0.57
Ice-10.10	46.81	1.14	14.68	0.13	10.47	0.16	11.28	12.49	1.65	0.18	0.18	99.2	0.31 ± 0.007	170 ± 22	88.9 ± 1.8	3360 ± 800	106 ± 11
Ice-10.11a	47.76	1.49	12.49	0.08	13.32	0.21	11.87	10.31	1.86	0.3	0.27	100.0	0.51 ± 0.01	644 ± 58	174 ± 3.9	1200 ± 40	147 ± 15
Ice-10.11b	47.74	1.57	12.99	0.06	12.9	0.21	10.94	10.72	2.06	0.29	0.22	99.7	0.40 ± 0.008	301 ± 27	178 ± 3.5	1100 ± 35	148 ± 15
Ice-10.12	46.97	1.21	12.87	0.08	11.04	0.18	12.59	11.85	1.67	0.14	0.16	98.8	0.68 ± 0.01	31.0 ± 3.2	64.9 ± 1.2	859 ± 27	67.8 ± 7.0
Ice-10.13	47.26	1.38	12.89	0.08	11.63	0.19	12.64	10.46	1.85	0.18	0.15	98.7	0.47 ± 0.01	32.7 ± 4.5	106 ± 3.7	927 ± 33	81.3 ± 8.8
Ice-10.14	49.44	0.49	16.98	0.5	9	0.15	7.85	13.43	2.18	0.01	0.02	100.1	0.61 ± 0.01	505 ± 64	65.2 ± 1.2	535 ± 19	1.62 ± 0.17
Ice-10.15	45.96	1.09	14.43	0.07	10.34	0.17	11.46	13.67	1.33	0.14	0.19	98.9	0.90 ± 0.02	103 ± 11	76.2 ± 2.1	1170 ± 39	64.5 ± 6.7
Ice-10.16	47.87	0.53	14.43	1.02	9.61	0.16	12.51	12.8	1.27	0	0.04	100.2	0.51 ± 0.01	30.3 ± 9.7	55.8 ± 1.2	285 ± 9.0	1.15 ± 0.16
Ice-10.17	47.82	1	13.5	0.06	10.48	0.17	12.86	12.68	1.38	0.21	0.34	100.5	0.45 ± 0.009	38.7 ± 9.3	61.7 ± 1.3	854 ± 27	96.7 ± 9.9
Ice-10.19a	47.38	1.43	12.47	0.06	11.03	0.19	15.04	9.97	1.97	0.35	0.1	100.0	0.54 ± 0.01	33.3 ± 2.2	151 ± 6.6	983 ± 36	223 ± 25
Ice-10.19b	47.39	1.56	14.19	0.05	10.93	0.21	10.16	12.89	1.74	0.23	0.02	99.4	0.80 ± 0.02	801 ± 800	88.8 ± 4.1	884 ± 35	127 ± 15
Ice-10.20	46.94	0.64	14.17	0.09	8.99	0.18	15.69	11.58	1.51	0.02	0	99.8	0.18 ± 0.004	203 ± 44	46.9 ± 2.8	123 ± 7.0	60.5 ± 7.6
Ice-10.21a	48.47	0.57	14.05	0.04	9.97	0.15	12.49	12.91	1.58	0.04	0	100.3	0.51 ± 0.01	28.5 ± 3.6	68.2 ± 3.1	715 ± 27	17.4 ± 2.0
Ice-10.21b	48.45	0.69	14.3	0.06	10.22	0.21	11.69	13.38	1.45	0.06	0	100.5	0.62 ± 0.01	35.9 ± 4.2	75.2 ± 3.2	714 ± 26	23.4 ± 2.7
Ice-10.22	47.65	0.79	13.13	0.09	11.49	0.21	10.97	12.52	3.33	0.06	0	100.2	0.90 ± 0.01	1330 ± 1500	481 ± 21	556 ± 20	115 ± 13
Ice-10.23	45.62	0.66	15.36	0.75	10.68	0.21	9.94	13.31	3.33	0.03	0	99.9	0.85 ± 0.01	692 ± 59	3640 ± 150	597 ± 21	467 ± 53
Ice-10.24	48.27	1.39	13.78	0.04	10.51	0.21	12.48	12.1	1.59	0.17	0.12	100.7	0.54 ± 0.01	27.9 ± 2.6	69.8 ± 3.0	837 ± 30	74.2 ± 8.4
Ice-10.25a	47.99	1.77	13.43	0.03	12.77	0.23	9.82	11.7	2.01	0.31	0.19	100.3	0.64 ± 0.02	36.8 ± 3.2	173 ± 8.0	1120 ± 42	155 ± 18
Ice-10.25b	47.15	1.47	12.52	0.05	13.05	0.26	11.45	11.1	1.64	0.32	0	99.0	0.64 ± 0.01	51.4 ± 3.2	151 ± 6.6	1070 ± 39	176 ± 20
Ice-11.1	48.94	0.72	16.2	0.07	8.52	0.16	11.17	13.3	1.47	0.1	0.15	100.8	0.55 ± 0.01	31.3 ± 4.5	75.7 ± 2.1	301 ± 29	1.12 ± 0.13
Ice-11.2	47.9	1.37	14.54	0	9.86	0.17	11.71	13.41	1.35	0	0.16	100.5	0.41 ± 0.009	181 ± 20	46.8 ± 0.89	610 ± 19	42.1 ± 4.4
Ice-11.3	47.65	0.72	14.23	1.12	10.1	0.19	11.44	14.26	1.67	0	0.11	101.5	0.62 ± 0.01	424 ± 43	48.3 ± 1.0	482 ± 15	3.73 ± 0.39
Ice-11.4	47.36	0.59	14.12	1.74	10.3	0.15	14.13	11.53	1.79	0	0.1	101.8	0.43 ± 0.009	99.4 ± 13	51.4 ± 0.94	292 ± 9.2	4.40 ± 0.46

Table 4: (Continued). Major oxide and volatile data for all melt inclusions analyzed in this study. Major oxides and H_2O concentrations are in wt. %. Carbon, F, S, and Cl concentrations are ppm. 2σ uncertainties are shown for volatile data.

Sample	SiO_2	TiO_2	Al_2O_3	Cr_2O_3	FeO	MnO	MgO	CaO	Na_2O	K_2O	SO_3	Total	H_2O (wt%)	C (ppm)	F (ppm)	S (ppm)	Cl (ppm)
Ice-11.5	48.04	1.16	15.04	0.73	7.05	0.11	14.39	13.38	1.73	0	0.09	101.7	0.31 ± 0.006	220 ± 22	43.7 ± 0.82	300 ± 9.5	8.27 ± 0.86
Ice-11.6	48.27	0.55	14.63	0.79	8.38	0.12	14.16	12.83	1.69	0.01	0.15	101.6	0.35 ± 0.008	0.183 ± 5.4	53.0 ± 1.1	347 ± 11	1.19 ± 0.14
Ice-11.7	49.11	0.81	15.44	0.18	8.05	0.12	11.52	13.93	1.54	0	0.1	100.8	0.34 ± 0.007	0.199 ± 30	68.1 ± 1.3	309 ± 9.8	1.55 ± 0.18
Ice-11.8a	48.1	0.6	13.78	1.47	8.83	0.14	15.1	12.38	1.64	0.01	0.07	102.1	0.49 ± 0.01	183 ± 17	59.0 ± 1.3	269 ± 27	6.12 ± 0.64
Ice-11.8b	50.34	0.57	15.19	0.8	8.92	0.16	8.68	13.81	1.55	0	0.1	100.1	1.2 ± 0.05	535 ± 120	86.3 ± 2.7	312 ± 16	5.83 ± 0.62
Ice-11.9a	47.2	0.67	13.8	1.1	10.4	0.15	14.74	11.56	1.91	0	0.08	101.6	0.51 ± 0.01	590 ± 75	49.4 ± 1.1	303 ± 9.9	5.93 ± 0.71
Ice-11.9b	48.15	0.68	15.08	1.58	10.25	0.15	10.88	12.64	1.45	0.01	0.1	101.0	0.58 ± 0.01	72.7 ± 11	59.8 ± 1.2	315 ± 16	1.06 ± 0.27
Ice-11.10	48.04	0.72	15.13	0.79	8.21	0.16	11.98	14.48	1.66	0	0.18	101.4	0.78 ± 0.02	1300 ± 3000	59.7 ± 1.2	224 ± 9.6	4.93 ± 3.7
Ice-11.11	48.13	0.65	14.97	1.71	9.09	0.16	11.25	13.74	1.7	0	0.12	101.5	0.47 ± 0.01	72.9 ± 7.7	58.1 ± 1.2	469 ± 15	1.57 ± 0.19
Ice-11.12a	48.31	0.66	14.68	1.72	9.73	0.13	12.05	13.03	1.63	0.04	0.12	102.1	0.49 ± 0.01	77.3 ± 7.2	58.2 ± 1.2	450 ± 14	1.61 ± 0.18
Ice-11.12b	47.3	0.74	14.53	0.96	9.63	0.14	13.55	12.1	1.88	0.01	0.13	101.0	0.39 ± 0.008	361 ± 33	85.4 ± 1.6	345 ± 11	16.9 ± 1.7
Ice-11.13	48.1	0.78	15.36	1.12	7.72	0.15	13.03	13.08	1.79	0.05	0.24	101.4	0.33 ± 0.007	77.4 ± 7.8	60.3 ± 1.1	415 ± 13	1.53 ± 0.18
Ice-11.14a	45.72	0.83	13.92	1.25	11.15	0.16	14.13	12.51	1.2	0.03	0.12	101.0	0.57 ± 0.01	168 ± 25	71.8 ± 1.3	721 ± 65	28.0 ± 2.9
Ice-11.14b	44.77	0.91	15.08	0.78	10.95	0.18	11.87	15.32	1.73	0.03	0.1	101.7	0.67 ± 0.01	182 ± 25	68.3 ± 1.2	345 ± 13	22.1 ± 2.3
Ice-11.15a	46.98	0.96	14.44	0	10.04	0.17	13.09	13.09	1.64	0	0.12	100.5	0.74 ± 0.04	2240 ± 350	92.7 ± 4.6	333 ± 14	29.0 ± 3.5
Ice-11.15b	47.06	1.05	13.96	0.1	10.01	0.16	13.73	12.92	1.77	0	0.11	100.9	0.58 ± 0.01	76.9 ± 8.6	59.2 ± 1.3	417 ± 13	11.8 ± 1.2
Ice-11.15c	48.24	1.09	15.01	0	9.49	0.17	10.74	13.99	1.64	0	0.11	100.5	0.44 ± 0.01	40.1 ± 8.5	58.9 ± 1.2	355 ± 11	1.41 ± 0.19
Ice-11.15d	47.97	1.12	15.05	0.09	9.61	0.17	11.02	13.83	2.32	0.11	0.15	101.4	0.44 ± 0.01	38.3 ± 11	58.8 ± 1.1	346 ± 11	1.36 ± 0.16
Ice-16.1	46.53	1.1	15.15	0.42	12.54	0.24	13.19	9.89	2.32	0.11	0.15	101.6	0.41 ± 0.005	425 ± 100	220 ± 8.0	564 ± 14	41.9 ± 4.6
Ice-16.2a	47.54	2.09	14.4	0	12.18	0.19	10.3	11.93	2.16	0.12	0.23	101.1	0.49 ± 0.01	3110 ± 1100	256 ± 11	885 ± 35	60.4 ± 6.9
Ice-16.2b	45.36	1.63	12.95	0.19	12.25	0.21	13.97	10.29	1.75	0.13	0.23	99.0	0.32 ± 0.005	281 ± 68	249 ± 9.5	876 ± 23	48.6 ± 5.4
Ice-16.3	47.96	1.94	14.42	0	11.21	0.19	10.71	11.37	2.16	0.13	0.25	100.3	0.43 ± 0.007	666 ± 160	247 ± 9.2	1050 ± 26	54.3 ± 6.0
Ice-16.4	47.32	2.14	12.91	0.05	12.84	0.2	12.87	10.48	1.91	0.32	0.34	101.4	0.55 ± 0.008	110 ± 29	212 ± 8.2	1180 ± 32	161 ± 18
Ice-16.5	47.86	1.56	13.79	0.04	11.41	0.19	13.06	10.21	2	0.42	0.28	100.8	0.48 ± 0.007	98.5 ± 25	203 ± 7.8	863 ± 24	70.4 ± 7.9
Ice-16.6	47.43	1.93	14.81	0	11.18	0.2	10.56	11.59	2.25	0.17	0.25	100.4	0.42 ± 0.007	768 ± 180	251 ± 9.3	919 ± 24	55.7 ± 6.4
Ice-16.7a	46.2	1.66	14.21	1.53	13.1	0.24	12.15	10.77	1.93	0.17	0.22	102.2	0.51 ± 0.007	195 ± 57	284 ± 10	877 ± 24	62.5 ± 7.1
Ice-16.7b	47.54	1.63	13.94	0.15	12.75	0.21	10.78	11.6	2.09	0.15	0.2	101.0	0.52 ± 0.007	142 ± 35	248 ± 9.0	854 ± 21	70.0 ± 7.7
Ice-16.8	48.06	1.53	13.36	0.11	11.67	0.19	13.53	10	2.15	0.19	0.27	101.1	0.41 ± 0.005	40.4 ± 10	256 ± 9.4	973 ± 24	85.9 ± 9.5
Ice-16.9	44.4	2.51	13.72	0.02	11.99	0.18	11.15	10.87	1.95	0.3	0.44	97.5	0.59 ± 0.009	1990 ± 530	254 ± 9.3	1630 ± 51	185 ± 20
Ice-25.1	49.43	1.19	15.98	0.07	8.46	0.16	9.36	11.97	2.18	0.06	0.13	99.0	0.48 ± 0.01	22.4 ± 2.5	355 ± 17	663 ± 26	24.0 ± 2.7
Ice-25.2a	48.54	1.47	14.34	0.03	9.68	0.18	11.61	11.80	1.83	0.22	0.10	99.8	0.46 ± 0.008	0.00 ± 14	372 ± 16	766 ± 27	104 ± 12
Ice-25.2b	48.31	1.40	14.35	0.07	9.41	0.18	12.46	11.45	1.81	0.25	0.12	99.8	0.41 ± 0.008	27.3 ± 3.6	344 ± 15	805 ± 29	106 ± 12
Ice-25.3	47.61	1.39	14.11	0.04	9.88	0.16	12.78	11.45	2.01	0.20	0.13	99.8	0.53 ± 0.01	50.5 ± 4.9	391 ± 18	771 ± 29	74.6 ± 8.6
Ice-25.4	47.90	1.56	14.55	0.05	9.71	0.17	12.69	11.17	1.86	0.19	0.08	99.9	0.50 ± 0.009	31.1 ± 3.9	392 ± 17	790 ± 31	77.1 ± 8.7
Ice-25.5	47.44	1.43	13.43	0.06	10.40	0.18	12.81	11.33	1.75	0.17	0.06	99.1	0.77 ± 0.01	0.00 ± 40	348 ± 15	822 ± 30	66.7 ± 7.5
Ice-25.6	47.20	1.48	14.56	0.08	9.52	0.18	13.67	11.18	1.81	0.20	0.10	100.0	0.48 ± 0.01	31.3 ± 2.9	346 ± 15	688 ± 26	79.0 ± 8.9
Ice-25.7	47.18	1.43	13.29	0.04	10.80	0.19	13.62	11.02	1.74	0.15	0.09	99.6	0.66 ± 0.01	0.00 ± 36	345 ± 15	720 ± 26	67.3 ± 7.6
Ice-25.8	49.82	1.55	14.77	0.04	10.70	0.17	9.33	12.37	1.42	0.14	0.11	100.4	0.81 ± 0.02	41.0 ± 3.4	389 ± 17	794 ± 29	74.9 ± 8.5

Table 4: (Continued). Major oxide and volatile data for all melt inclusions analyzed in this study. Major oxides and H_2O concentrations are in wt. %. Carbon, F, S, and Cl concentrations are ppm. 2σ uncertainties are shown for volatile data.

Sample	SiO_2	TiO_2	Al_2O_3	Cr_2O_3	FeO	MnO	MgO	CaO	Na_2O	K_2O	SO_3	Total	H_2O (wt%)	C (ppm)	F (ppm)	S (ppm)	Cl (ppm)
Ice-25.9a	48.47	1.35	12.69	0.02	11.30	0.22	12.43	10.68	1.92	0.26	0.12	99.5	0.61 ± 0.01	16.0 ± 2.1	328 ± 15	847 ± 32	110 ± 13
Ice-25.9b	47.41	1.40	11.88	0.01	11.90	0.22	14.15	10.19	1.91	0.23	0.13	99.4	0.66 ± 0.01	19.1 ± 2.2	324 ± 14	922 ± 34	109 ± 12
Ice-25.9c	47.86	1.43	12.37	0.03	12.00	0.26	12.00	11.13	1.79	0.21	0.13	99.2	0.77 ± 0.02	26.7 ± 2.3	346 ± 16	990 ± 35	100 ± 11
Ice-25.10	47.80	1.20	13.28	0.03	9.77	0.20	15.09	10.21	1.65	0.21	0.10	99.5	0.47 ± 0.01	23.2 ± 2.5	316 ± 14	761 ± 28	88.1 ± 10
Ice-25.11	47.28	1.32	13.58	0.06	10.10	0.18	14.39	10.65	1.84	0.17	0.08	99.7	0.74 ± 0.01	32.4 ± 3.9	341 ± 14	752 ± 27	67.6 ± 7.6
Ice-25.12b	48.02	1.65	14.68	0.05	10.20	0.19	9.47	12.27	2.07	0.23	0.11	98.9	0.86 ± 0.01	29.0 ± 2.8	365 ± 15	779 ± 28	78.7 ± 8.9
Ice-25.12c	48.67	1.65	14.44	0.05	10.20	0.18	9.28	12.15	2.08	0.22	0.11	99.0	0.93 ± 0.02	32.2 ± 3.1	373 ± 17	855 ± 31	88.6 ± 10
Ice-25.12d	47.76	1.39	12.59	0.04	10.50	0.20	13.63	11.02	1.85	0.20	0.09	99.3	0.76 ± 0.02	21.8 ± 2.6	339 ± 15	755 ± 29	82.0 ± 9.4
Ice-25.13	49.30	0.38	12.68	0.06	8.97	0.14	16.34	9.61	1.73	0.02	0.02	99.2	0.78 ± 0.01	164 ± 10	1220 ± 51	314 ± 11	44.7 ± 5.0

A.

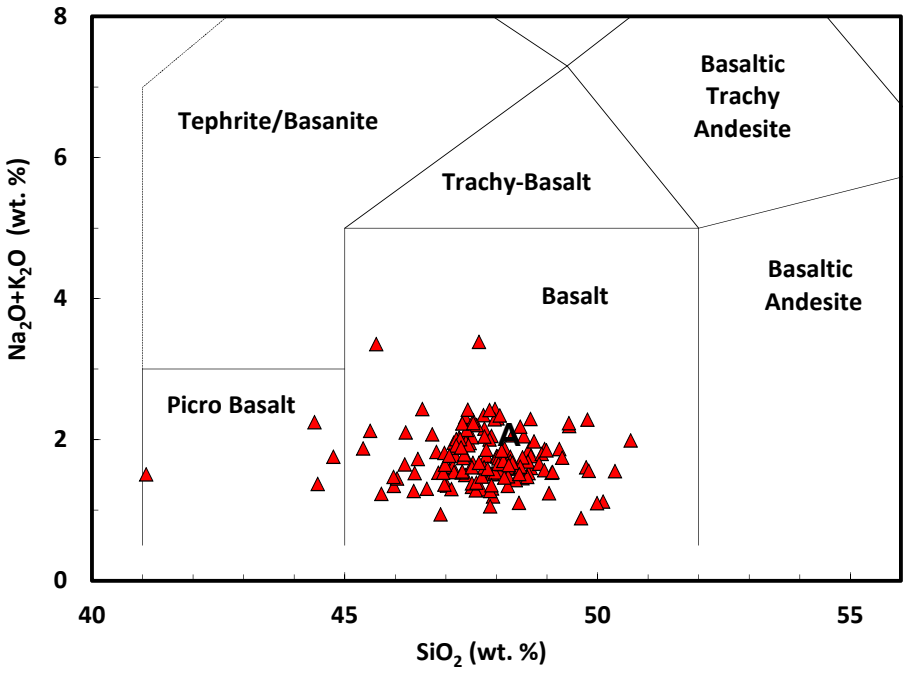

B.

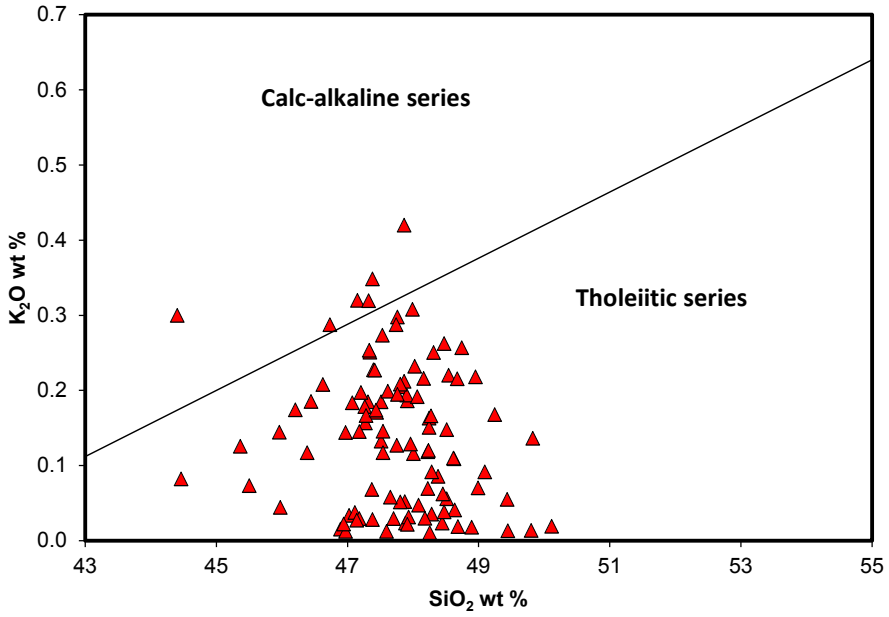

Figure 3: (A) Total alkali silica diagram showing magma compositions for studied melt inclusions. (B) K_2O as a function of SiO_2 showing the boundary between alkaline and tholeiite compositions for Reykjanes Peninsula melt inclusions analyzed in this study (series boundary defined by Peccerillo and Taylor 1976).

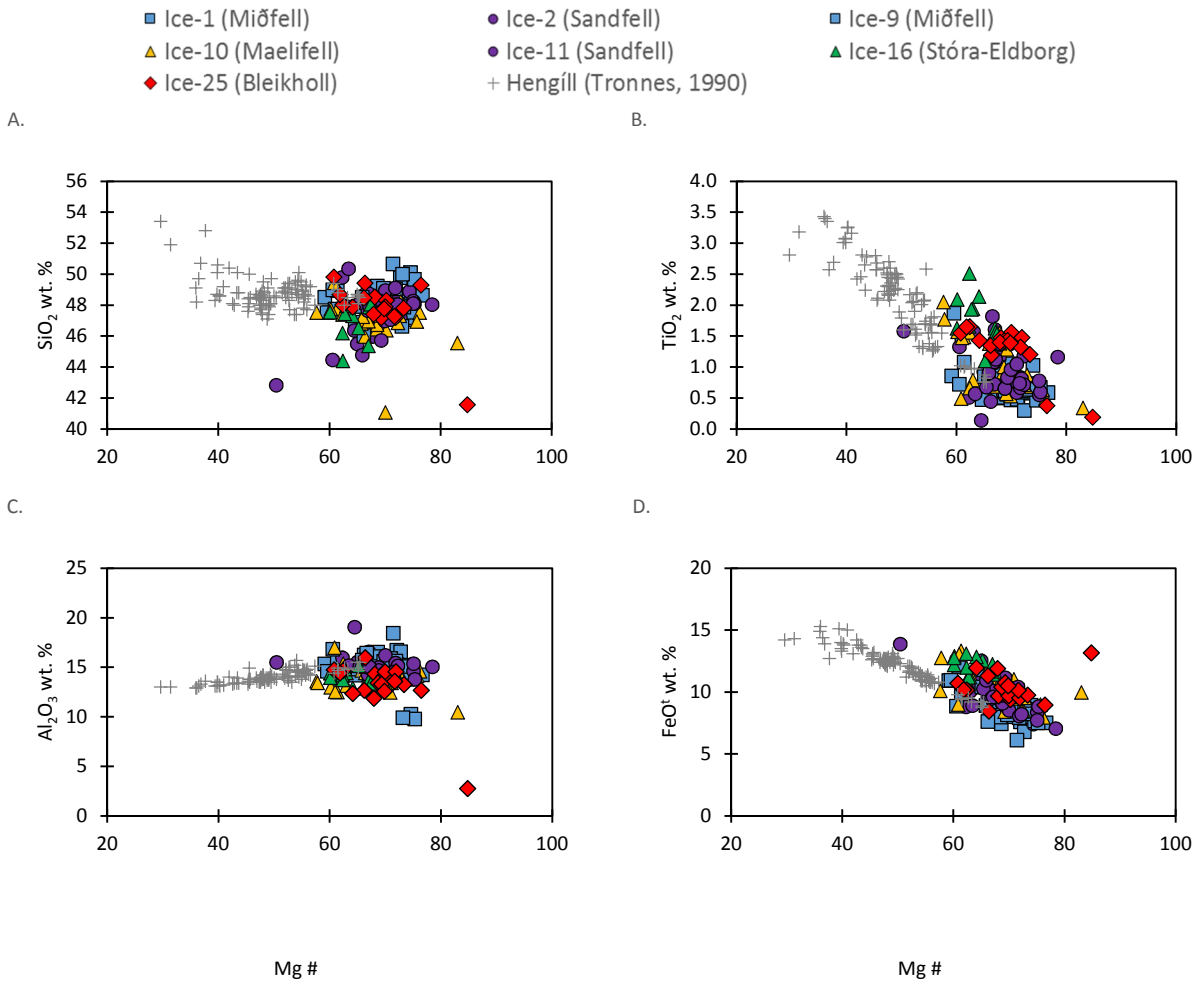

Figure 4: Major oxides vs. Mg # (mol %) for studied melt inclusions compared with data for volcanic glasses in the Hengill Swarm analyzed by Tronnes (1990).

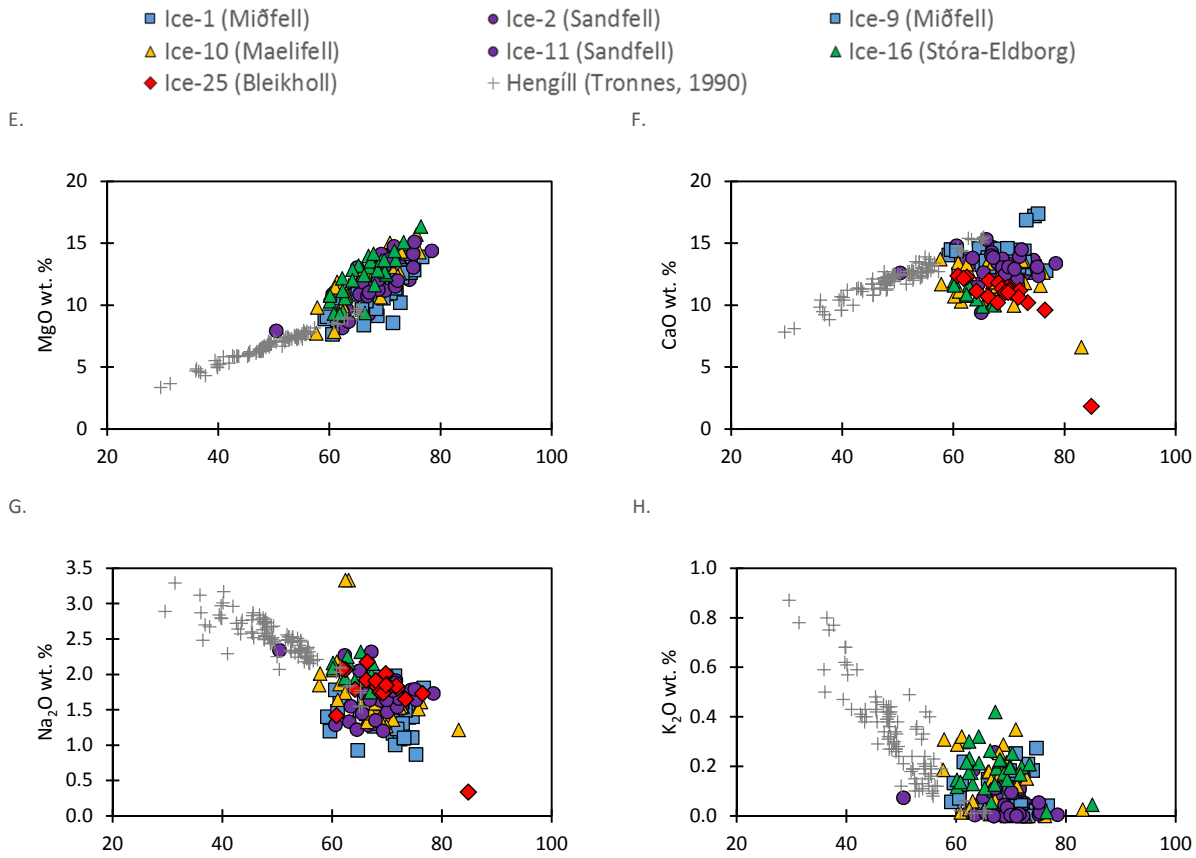

Figure 4: (Continued). Major oxides vs. Mg # (mol %) for studied melt inclusions compared with data for volcanic glasses in the Hengill Swarm analyzed by Tronnes (1990).

4.3 Water in Melt Inclusions

Measured H_2O concentrations in the studied melt inclusions show a range of concentrations from 0.17 wt. % to a maximum value of 1.99 ± 0.06 wt. % (Table 4). The maximum values exceed the H_2O concentrations reported by Nichols et al. (2002) for basaltic glass, but a majority of the melt inclusions preserve volatile concentrations in general agreement with previously reported data for the Reykjanes Peninsula (e.g., Sigvaldson and Oskarsson, 1976; Schilling et al., 1980; Jambon et al., 1995; Nichols et al., 2002).

The two highest H_2O concentrations reported in this study occur in intraglacial picrites from Sandfell in the Hengíll swarm, 1.99 wt. % (*Ice-2)* and 1.22 wt. % (*Ice-11).* Another intraglacial picrite located in the Hengíll swarm at Mælifell, *Ice-10,* has a maximum H_2O concentration of 0.90 wt. % (Table 4). Maximum H_2O concentrations in the intraglacial picrites from Miðfell, also located in the Hengíll swarm, are lower than those from Sandfell and Mælifell. The Miðfell samples have maximum concentrations of 0.61 wt. % *(Ice-1)* and 0.78 wt. % *(Ice-9.)* Water concentrations in the late glacial olivine-tholeiite from Bleikholl, *Ice-25,* located in the Grindavík swarm*,* reach a maximum value of 0.93 wt. %. The postglacial olivine-tholeiite from Stora-Eldborg in the Krýsuvík swarm, *Ice-16*, has the lowest maximum H_2O concentration of 0.59 wt. %. For the samples studied, H_2O concentrations generally decrease with increasing distance from the plume head – located beneath Vatnajökull Glacier (Wolfe et al., 1997) – as noted previously by Nichols et al. (2002).

Figure 5 shows the relationship between major-oxide and H_2O concentrations for melt inclusions in this study. In general, the H_2O concentrations are not correlated with major oxides.

The lack of correlation suggests that H_2O is not being concentrated in the melt during crystallization (Section 5.1). Additionally, water concentrations do not correlate with K_2O (Figure 5h), a similarly incompatible element.

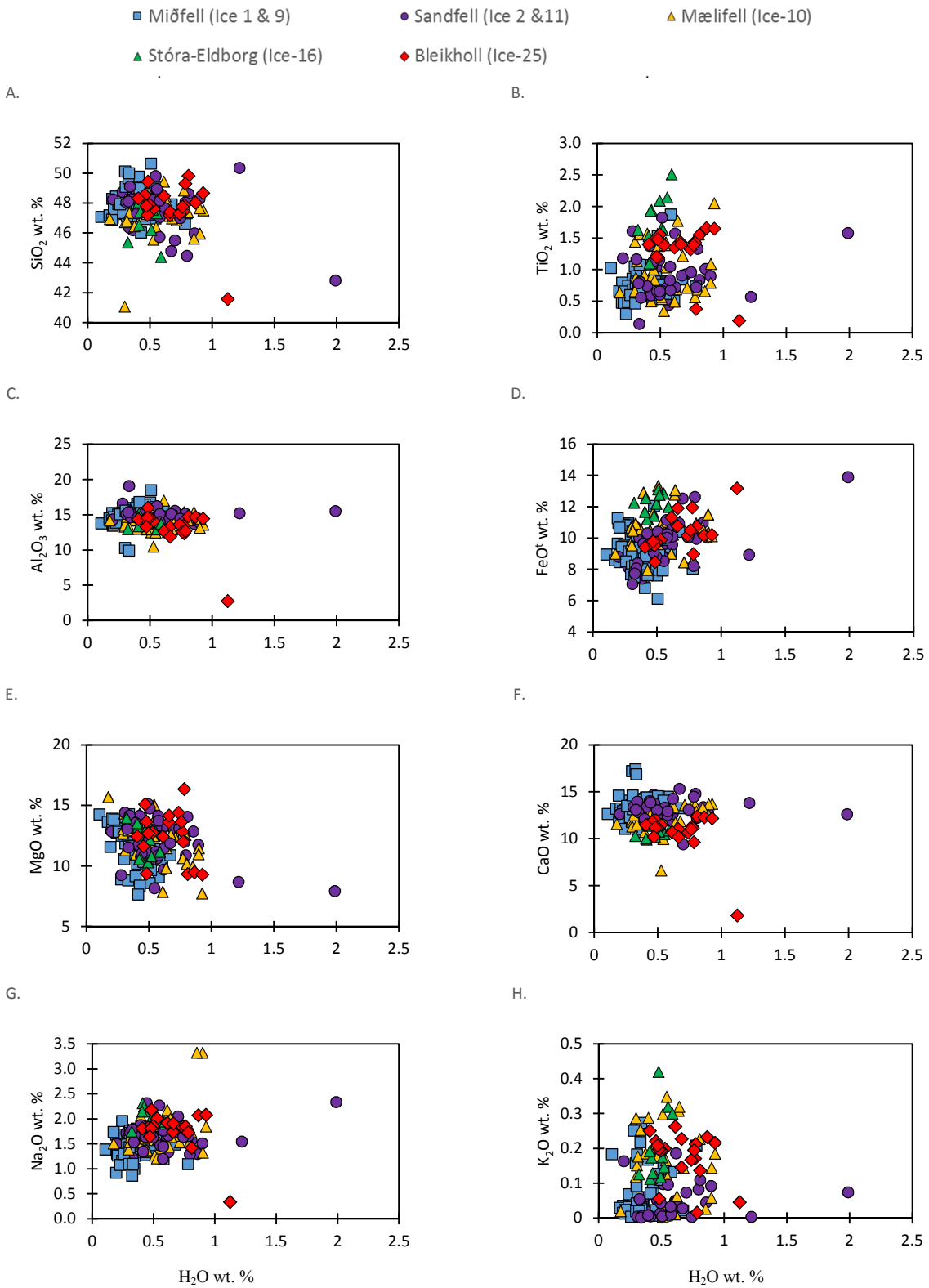

Figure 5*:* Harker-style plots showing major oxides as a function of H_2O compositions for the studied Reykjanes Peninsula melt inclusions. Samples are grouped by location and corresponding sample numbers are shown for reference.

4.4 Carbon Dioxide, F, S, and Cl in Melt Inclusions

Carbon dioxide, F, S, and Cl for the Reykjanes Peninsula melt inclusions studied here are heterogeneous (Figure 6; Table 4) and exhibit a wide range of concentrations suggesting a complex history of degassing, magmatic differentiation, and post-entrapment modification. However, a few trends providing coherent correlations with other elements remain and offer some useful insights. Volatile abundances show significant scatter as a function of H_2O abundance (Figure 6) and trends are restricted to individual sample locations. Carbon dioxide abundances show little to no correlation with H_2O but in some sample locations, such as Miðfell, CO_2 generally decreases with increasing H_2O (Figure 6.A). Fluorine concentrations appear to covary with H_2O, and increase with increasing H_2O (Figure 6.B). Fluorine concentrations are greatest in the olivine tholeiites from Bleikholl and Stora-Eldborg. Sulfur and Cl lack any correlation with H_2O (Figure 6.C and 6.D).

Sulfur concentrations and S solubility are functions of temperature, composition, fugacity, pressure, and degassing (e.g., Wallace and Carmichael, 1992; Wallace and Edmond, 2011; Bucholz et al., 2013). The Reykjanes Peninsula samples represent a wide range of compositions (S = ~220-1600 ppm) suggesting variable degrees of degassing and entrapment at a variety of pressures. Sulfur concentrations generally increase as FeO^t increases from 7.05-13.88 wt. % (Figure 7). A majority of these data plot below but parallel the empirical sulfide saturation curve (Mathez, 1976) and sulfide saturation models (e.g., Wallace and Carmichael, 1992; Wallace and Edmond, 2011) and represent uncompromised melt inclusions. MORB glasses typically have S concentrations of >1000 ppm. Conversely, lavas erupted in subaerial and shallow submarine settings show S < 250 ppm (Davis et al. 1991). There is a lack of correlation between S and H_2O

in the Reykjanes Peninsula samples (Figure 6c), and significant scatter in the data suggesting S loss at low pressures (e.g., Wallace and Edmond, 2011).

Chlorine concentrations in Reykjanes Peninsula melt inclusions show a range of concentrations (~1-223 ppm, one outlier = 467 ppm) and several of the samples have Cl concentrations lower than the lowest standard used for calibration (Alvin 519-4-1, Cl=45 ppm). Fifty eight of the melt inclusions studied here have Cl concentrations < 20 ppm, these are amongst the lowest Cl concentrations reported for Iceland. However, several of the values fall within the range of previously reported data for Iceland and the Northern MAR (e.g., Sigvaldson and Oskarsson, 1976; Schilling et al., 1980; Metrich et al., 1991; Jambon et al., 1995), 20-50 ppm for primitive MORB (Michael and Schilling, 1989) and 29-61 ppm for WVZ samples from Iceland (Licciardi et al., 2008).

Dixon and Clague (2001) modeled the behavior of Cl as a function of the degree of melting using SiO_2 as a proxy because the highly incompatible nature of Cl implies its concentrations should increase with decreasing extents of melting and increasing extents of crystallization. There is no correlation between SiO_2 and Cl in the Reykjanes Peninsula samples studied here. Similarly, the Cl concentrations show no correlation with MgO, an indication that Cl is not being concentrated during fractional crystallization (Michael and Cornell, 1998). When Cl is plotted against K_2O, a similarly incompatible element (Dixon and Clague, 2001; Figure 8), a positive correlation between the elements is observed and the slope of the regression line is ~0.046 (R^2 =0.82 excluding two outliers), consistent with the nearly constant Cl/K ratio of 0.05 for Iceland samples observed by Jambon et al. (1995).

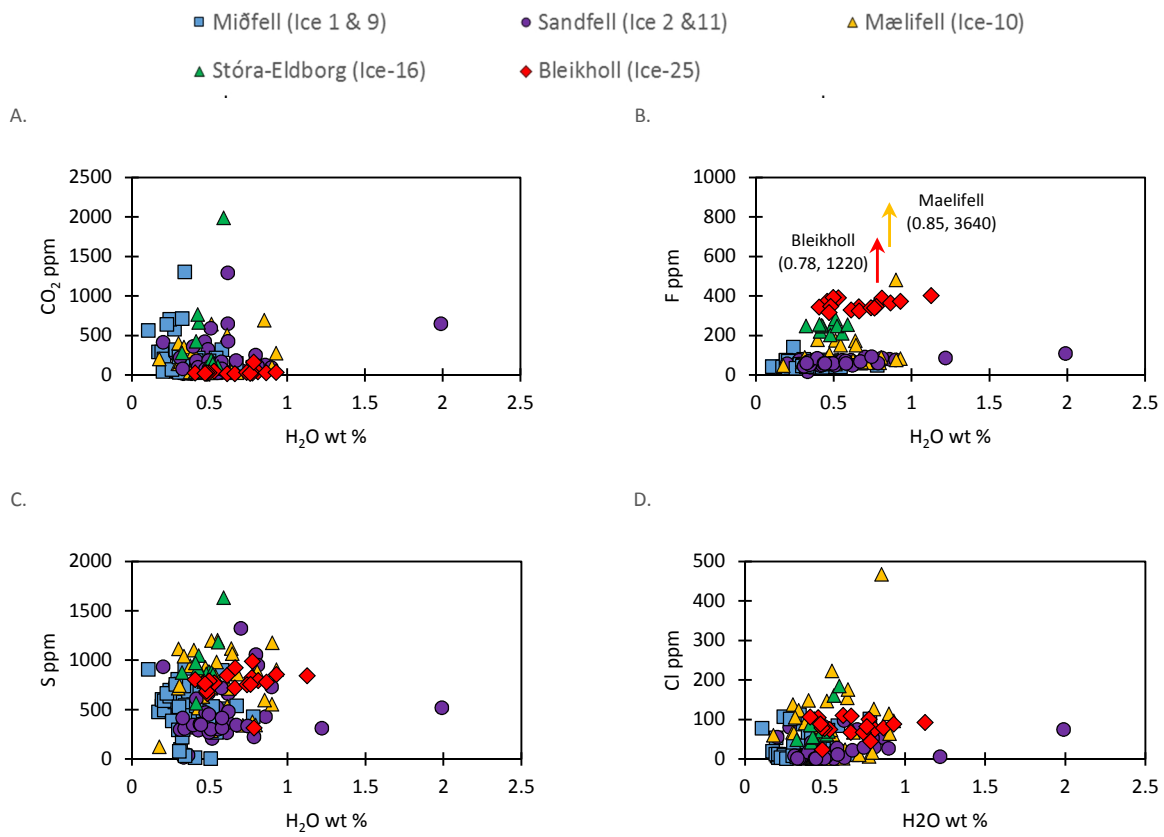

Figure 6: Volatile compositions (C, F, S, and Cl) as a function of H_2O. Carbon shows a general decrease with increasing H_2O (A). Fluorine and S show a general increase with increasing H2O concentrations (B, C). Significant scatter in all volatile species is observed.

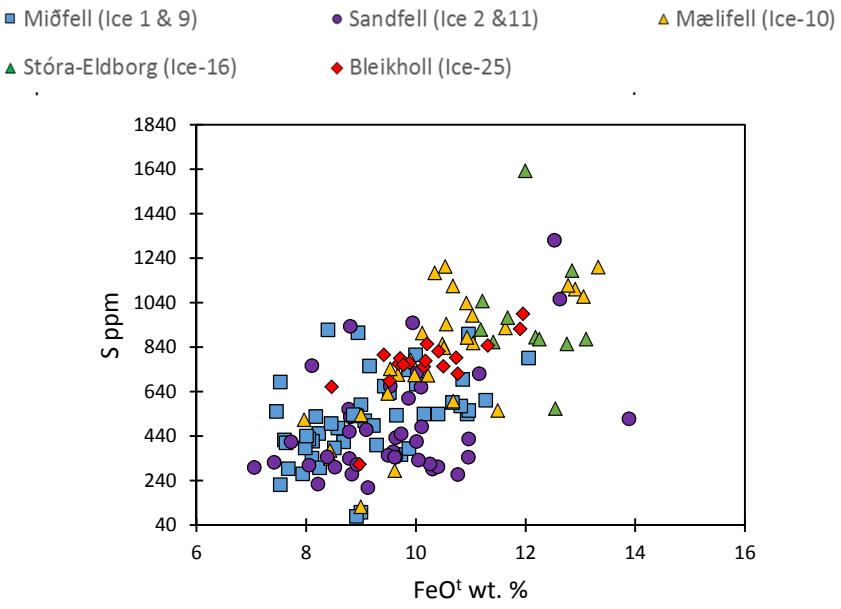

Figure 7: Sulfur concentrations as a function of FeO^t for all melt inclusions studied. Degassing of sulfur is likely, however the covariation of S and FeO suggests most samples were sulfide saturated, and minimal post entrapment modification occurred.

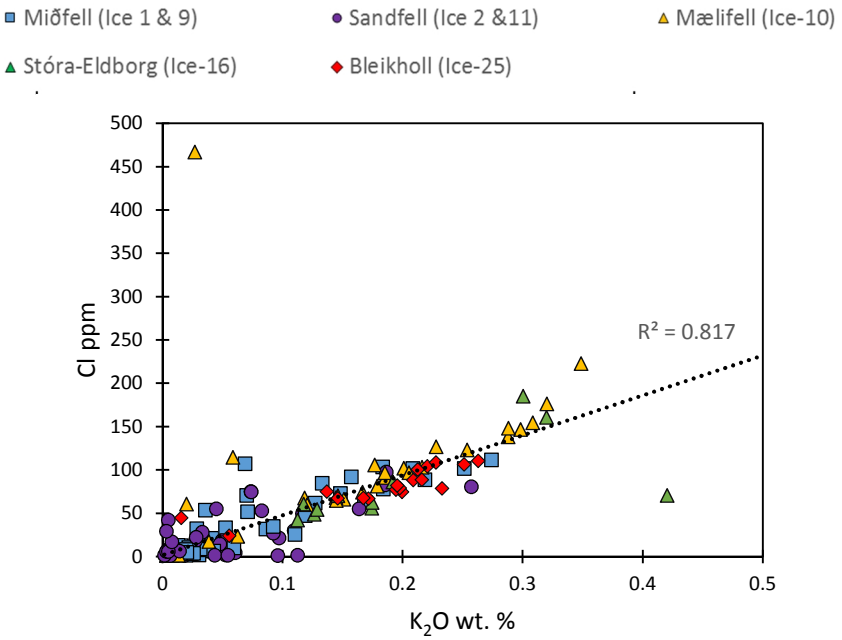

Figure 8: Cl concentrations as a function of K_2O for studied melt inclusions. Trend line excludes high Cl sample.

5. DISCUSSION

5.1 Degassing and Crystallization

Degassing, crystallization, and post-entrapment re-equilibration are processes that affect volatile abundances in melt inclusions as the host olivine ascends and eventually erupts at the surface (e.g., Danyushevsky et al., 2000; 2002; Métrich and Wallace, 2008; Johnson et al., 2010). For instance, melt inclusions trapped at different times and depths within the magmatic system should each record a unique melt composition. Re-equilibration of the melt inclusion with the host olivine at lower temperature may lead to FeO^t loss and MgO gain in the melt inclusion to high Mg olivine (Danyushevsky et al., 2000; 2002). Conversely, re-equilibration of the melt inclusion with the host-olivine grain at high temperatures may lead to MgO loss and FeO^t gain (Danyushevsky et al., 2000; 2002). In order to discern the relationship between volatile concentrations and noble gas signatures in the Reykjanes Peninsula samples, it is necessary to determine the extent to which volatile concentrations have decreased as a consequence of degassing or, conversely, increased due to crystallization processes or post-entrapment re-equilibration.

The loss of volatiles by degassing may be compensated by an increase of volatiles in the residual melt during crystallization (e.g., Jambon et al., 1995; Jonhnson et al., 2010; Wallace and Edmond, 2011). Dixon and Clague (2001) noted that degassing is a two-stage process; in the first stage, CO_2 is exsolved from the melt within the magma reservoir. Subsequently, in the second stage, H_2O, S, Cl and CO_2 are removed during typical eruption-related venting of gases (Dixon and Clague, 2001). The studied Reykjanes Peninsula melt inclusions display a wide range of H_2O and CO_2 concentrations indicating that melt-inclusion entrapment occurred over a range of

pressures. The vapor-saturation pressure of a melt inclusion can be estimated using its H_2O and CO_2 concentrations (e.g., Dixon, 1997; Newman and Lowerstern, 2002).

Calculated vapor-saturation pressures for the CO_2 and H_2O concentrations of the studied melt inclusions using VolatileCalc, calibrated for tholeiitic to silica-undersaturated compositions (Newman and Lowenstern, 2002), yields entrapment pressures <10 to 300 Mpa (Figure 9). The observed variability in H_2O and CO_2 concentrations in concert with calculated vapor-saturation pressures indicates that partially degassed melts were trapped as magma ascended through the crust. The loss of CO_2 relative to H_2O can be modeled using open-system degassing for the maximum measured H_2O concentration of 1.99 wt. % (Figure 9). Some of the data can be modeled by invoking closed-system degassing. In the closed-system-degassing model, a fluid with 3 wt. % H_2O is exsolved (Figure 9). Globally, closed-system degassing is true for several volcanoes as indicated by their melt inclusion data (Metrich and Wallace, 2008). However, the maximum H_2O concentrations of the Reykjanes Peninsula melt inclusions can be explained by closed-system degassing only if the initial H_2O concentration was significantly greater than the maximum value reported here. Certain melt inclusions appear to be in equilibrium with CO_2-rich fluids, as indicated by the isopleths in Figure 9. While the degassing paths and vapor-equilibrium models are speculative, it is clear that the melt inclusions are generally degassed to various degrees.

Volatiles are incompatible during melting and their concentrations may increase during fractional crystallization (Johnson et al., 2010). Therefore, the possibility that volatiles were concentrated in the melt inclusions leading to variations in volatile concentrations must be evaluated. First-order observations of the relationship between H_2O and other incompatible elements such as TiO_2, Na_2O, and K_2O reveal a lack of correlation (Figure 5). The absence of a negative correlation between H_2O and other incompatible elements coupled with the observed

enrichments of TiO_2, Na_2O, and K_2O at lower H_2O concentrations (Figure 5) suggests that H_2O is not being concentrated during crystallization but is degassing concurrently with crystallization (Cabato et al., 2015).

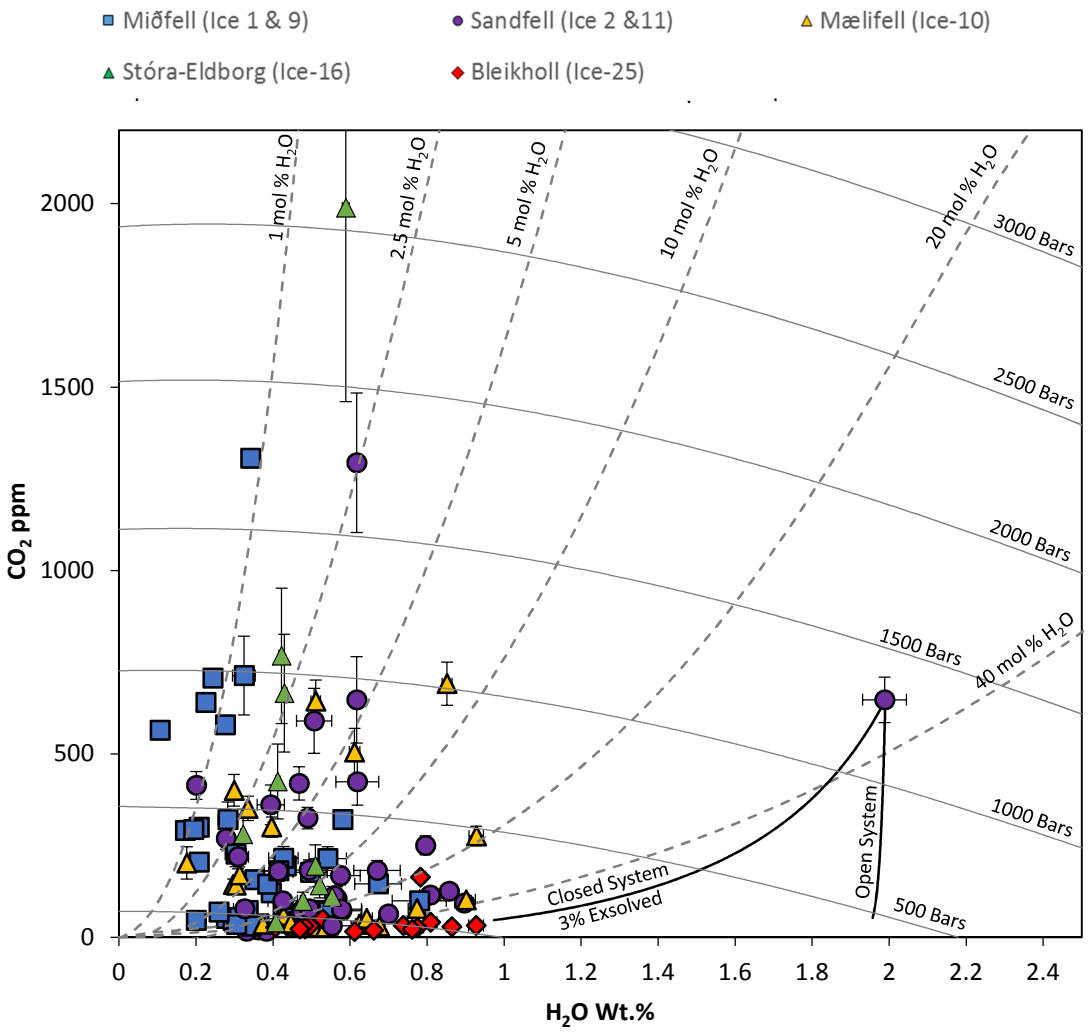

Figure 9: Melt Inclusion CO_2 vs. H_2O for the Reykjanes Peninsula melt inclusions analyzed in this study. Also shown are calculated vapor saturation isobars, open and closed system degassing paths, and isopleths all calculated using VolatileCalc (Newman and Lowernstern, 2002). Absolute 2σ uncertainties are shown, for several samples error bars are within symbol. Calculations were made using the average SiO_2 composition of 47.77 wt. % and a temperature of 1200^{O} C.

5.2 Source Lithology

Magma compositions can yield valuable information about the depth of melt extraction from the mantle (Lee et al., 2009). Koornneef et al. (2012) suggested that the observed trace element and Nd-Hf-Sr-Pb isotopic heterogeneity in Icelandic magmas can be explained by polybaric melting and melt extraction at variable depths from two components, an N-MORB and an enriched ancient recycled crustal component. Recent studies have invoked a peridotite-pyroxenite mantle beneath Iceland as a source for heterogeneity in the magmas (Shorttle and Maclennan, 2011; Koornneef et al., 2012).

Using the barometric model presented in Lee et al. (2009), the pressure and depth of mantle melt extraction has been calculated for the maximum H_2O concentrations reported in this study (Figure 10). The model presented in Lee et al. (2009) is calibrated for melts with SiO_2 concentrations greater than 43 wt. %; consequently the Sandfell sample Ice-2 could not be modelled because of the low SiO_2 concentration (42.82 wt. %) in the melt inclusion. For the remaining samples, maximum H_2O concentrations correlate with pressure along two trends. The Mælifell, Stora-Eldborg, Bleikholl, and Sandfell (Ice-ll) samples define one trend ($R^2 = 0.96$). The two Miðfell samples diverge from the trend defined by Mælifell, Stora-Eldborg, Bleikholl, and Sandfell to lower H_2O concentrations at a given pressure. The variation between the Miðfell samples and samples from the other four localities studied may be the result of melting two different mantle lithologies, peridotite and pyroxenite, as suggested by Shorttle and Maclennan (2011), and Koornneef et al. (2012). Melting commences at different temperatures and, consequently pressures, for pyroxenite and peridotite (Hirschmann et al., 2003; Koornneef et al.,

2012), with derivative melts having a variety of compositions. It is possible that the Mælifell, Stora-Eldborg, Bleikholl, and Sandfell samples are the results of melt extraction at different pressures from a pyroxenite source that began melting deeper in the mantle. Alternatively, the Miðfell samples could be the product of melt extraction from a peridotite source at shallower depths in the mantle.

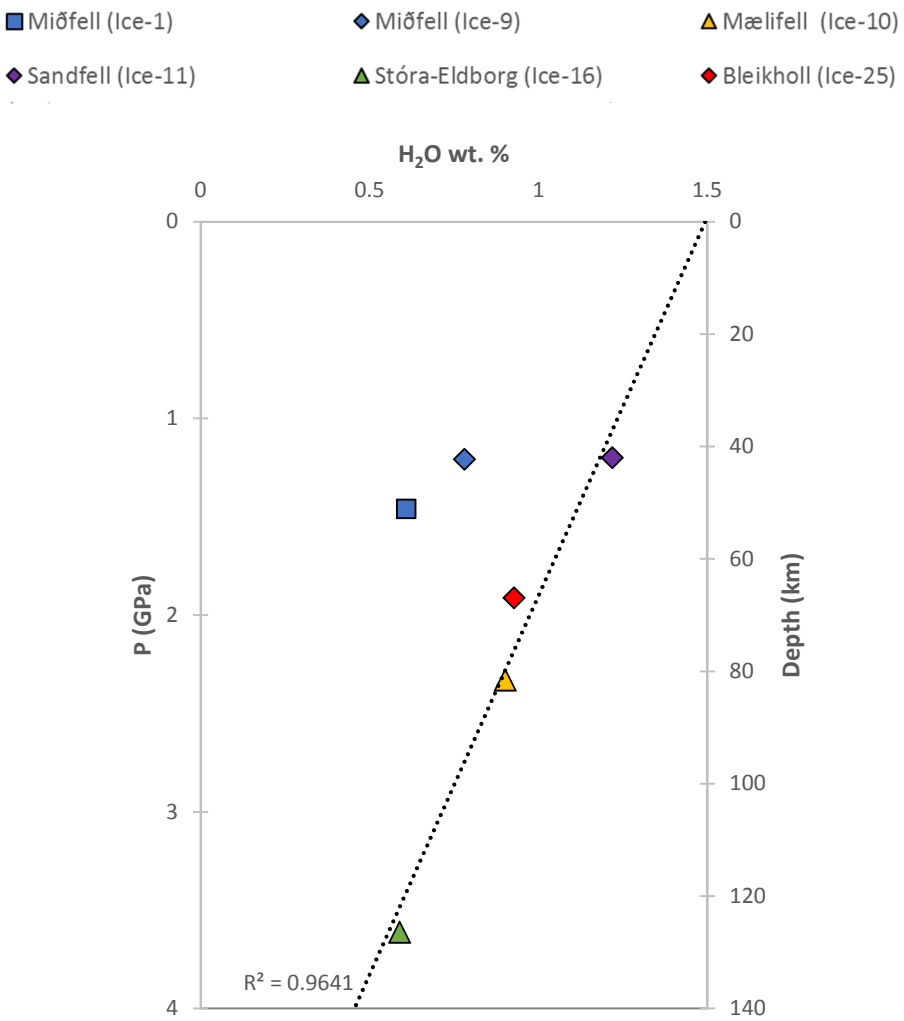

Figure 10: Water concentration as a function of depth and average pressure using melt inclusions with maximum H_2O concentrations. Regression line does not include the Miðfell samples as they appear to form their own trend. Ice-2 is not included, see text for discussion.

5.3 Volatiles and Noble Gases

A unique aspect of this study is that the volatile data reported here are from olivine-hosted melt inclusions belonging to the same sample suite used to study He and Ne isotopic compositions by Dixon et al. (2000) and Dixon (2003). This allows for a comparison of the new volatile data to the existing He and Ne isotopic signatures for the same sample. Several studies have shown that noble gas isotopic compositions and relative abundances can vary between individual flow units in sample sites distributed through Iceland and that the observed variations are representative of mantle heterogeneities (Harrison et al., 1999; Dixon et al., 2000; Trieloff et al., 2000; Moreira et al., 2001; Dixon, 2003; Licciardi et al., 2006; Furi et al., 2010). To compare the volatile data from this study to the noble gas data from Dixon et al. (2000) and Dixon (2003), the maximum volatile concentrations, representative of the least degassed primary melts in the sample, are correlated to the He (R/R_a) and Ne isotopic signature (Table 5). If replicate analyses were made by Dixon et al. (2000) and Dixon (2003) the mean noble gas value was used in this comparison to the volatiles (Table 2).

The H_2O and S data reported here show a negative correlation (Figure 11 and Figure 12B) with the helium data ($R/R_a = (^3He/^4He_{sample})/(^3He/^4He_{atmosphere})$) reported by Dixon et al. (2000) and Dixon (2003). Discrepancies in trends between volatile species as a function of R/R_a within a sample may result from a complex degassing history and source heterogeneities. Regardless, a negative correlation between R/R_a and the volatile concentrations for H_2O and S exists (Figure 11 and Figure 12B). In the case of S (Figure 12B), the Sandfell and Stóra-Eldborg samples are not included in the trend calculation. Sulfur concentrations vary as a consequence of pressure,

fugacity, and composition (Wallace 2005; Bucholz et al., 2013). The high S content in the Stóra-Eldborg melt inclusion may be due to a higher oxygen fugacity relative to the majority of Reykjanes Peninsula melt inclusions examined in this study and is therefore treated as an outlier. On the other hand, the low S concentration in the Sandfell sample may represent a S undersaturated melt in regards to sulfide. If this is the case diffusive loss of S is not replenished (Bucholz et al., 2013) therefore the sample is treated as an outlier for comparison purposes.

There is no direct correlation between H_2O concentrations and the concentration of ^4He. However, the Reykjanes Peninsula samples have lower ^4He concentrations and higher H_2O concentrations than the samples reported for the Reykjanes Ridge by Hilton et al. (2000). This evidence suggests degassing of CO_2 and noble gases coupled with the presence of high magmatic H_2O concentrations in Reykjanes Peninsula magmas relative to Reykjanes Ridge magmas (Hilton et al., 2000). Furthermore, as suggested by Hilton et al. (2000), for samples at latitudes higher than 61.3°N along the Reykjanes Ridge, a decrease in R/R_a values towards MORB values coupled with increased H_2O concentrations may be the result of interactions between mantle-derived magmas and the crust.

Several studies have proposed binary mixing between a primitive plume component and MORB to describe the heterogeneity of noble gases in Iceland (Moreira et al., 2001; Dixon, 2003; Furi et al., 2010) and along the Reykjanes Ridge (Hilton et al., 2000). Binary mixing models for Iceland, based on the relationship between He and Ne isotopic compositions (Moreira et al., 2001; Dixon, 2003; Furi et al., 2010), require that either He is enriched in the MORB component relative to Ne or that the plume component is depleted in Ne relative to He (Furi et al., 2010). To demonstrate the relationship between Ne isotopic compositions and H_2O, we plot the Reykjanes Peninsula samples in three-neon-isotope space (e.g., Dixon et al., 2000; Dixon, 2003), and overlay

the H_2O concentrations for each sample (Figure 13). Two of the three lowest H_2O concentrations reported in this study are from samples with Ne isotopic compositions that have 2σ errors overlapping with the solar-atmosphere mixing line (See Dixon 2003). Conversely, the three highest H_2O concentrations are found in samples that have 2σ errors overlapping with the MORB-atmosphere mixing line (See Dixon 2003). The Mælifell sample, Ice-10, is indistinguishable from atmospheric Ne (Dixon 2003). This observation suggests that the MORB Ne end-member has incorporated a component containing higher H_2O concentrations relative to the mantle component found in the solar Ne end member. Since the R/Ra values corresponding to the samples on the MORB – atmosphere mixing line are all greater than the typical MORB R/Ra ratio of ~8 (Graham, 2002), these observations suggest a complex mixing of plume and MORB end members capable of producing the observed heterogeneities in volatiles and noble gases.

Table 5: Melt inclusions with maximum volatile compositions.

Sample No.	H_2O (wt%)	C (ppm)	F (ppm)	S (ppm)	Cl (ppm)
Ice-1.3d	0.24 ± 0.01	---*	141 ± 2.9	696 ± 34	107 ± 11
Ice-1.10a	0.34 ± 0.01	32.7 ± 4.0	44.1 ± 0.86	918 ± 190	112 ± 12
Ice-1.12	0.61 ± 0.01	48.6 ± 5.2	59.0 ± 1.1	510 ± 17	1.40 ± 0.15
Ice-1.16d	0.34 ± 0.01	1310 ± 120	45.7 ± 0.94	540 ± 17	33.1 ± 3.4
Ice-2.1	0.62 ± 0.01	1290 ± 190	67.0 ± 2.0	661 ± 21	97.4 ± 10
Ice-2.6	0.70 ± 0.02	63.4 ± 7.5	91.4 ± 2.3	1320 ± 43	74.8 ± 7.8
Ice-2.9c	1.99 ± 0.06	648 ± 62	110 ± 2.4	518 ± 20	74.5 ± 7.7
Ice-2.10b	0.49 ± 0.01	325 ± 29	62.4 ± 1.2	664 ± 21	82.9 ± 8.6
Ice-9.1	0.49 ± 0.01	31.6 ± 2.3	68.3 ± 5.7	401 ± 13	25.5 ± 3.0
Ice-9.4	0.78 ± 0.02	99.5 ± 18	49.3 ± 4.1	427 ± 14	101 ± 12
Ice-9.14	0.48 ± 0.01	51.2 ± 5.7	59.3 ± 1.1	791 ± 25	61.7 ± 6.3
Ice-9.15b	0.32 ± 0.01	714 ± 65	42.0 ± 0.81	221 ± 7.2	4.96 ± 0.52
Ice-10.11a	0.51 ± 0.01	644 ± 58	174 ± 3.9	1200 ± 40	147 ± 15
Ice-10.15	0.90 ± 0.02	103 ± 11	76.2 ± 2.1	1170 ± 39	64.5 ± 6.7
Ice-10.23	0.85 ± 0.01	692 ± 59	3640 ± 150	597 ± 21	467 ± 53
Ice-11.2	0.41 ± 0.01	181 ± 20	46.8 ± 0.89	610 ± 19	42.1 ± 4.4
Ice-11.8b	1.2 ± 0.05	535 ± 120	86.3 ± 2.7	312 ± 16	5.83 ± 0.62
Ice-11.9a	0.51 ± 0.01	590 ± 75	49.4 ± 1.1	303 ± 9.9	5.93 ± 0.71
Ice-11.14a	0.57 ± 0.01	168 ± 25	71.8 ± 1.3	721 ± 65	28.0 ± 2.9
Ice-16.2a	0.49 ± 0.01	---*	256 ± 11	885 ± 35	60.4 ± 6.9
Ice-16.9	0.59 ± 0.01	1990 ± 530	254 ± 9.3	1630 ± 51	185 ± 20
Ice-25.9a	0.61 ± 0.01	16.0 ± 2.1	328 ± 15	847 ± 32	110 ± 13
Ice-25.9c	0.77 ± 0.02	26.7 ± 2.3	346 ± 16	990 ± 35	100 ± 11
Ice-25.12c	0.93 ± 0.02	32.2 ± 3.1	373 ± 17	855 ± 31	88.6 ± 10
Ice-25.13	0.78 ± 0.01	164 ± 10	1220 ± 51	314 ± 11	44.7 ± 5.0

* Indicates rejected value due to fluctuations in secondary ion image for specific volatile species during SIMS analysis.

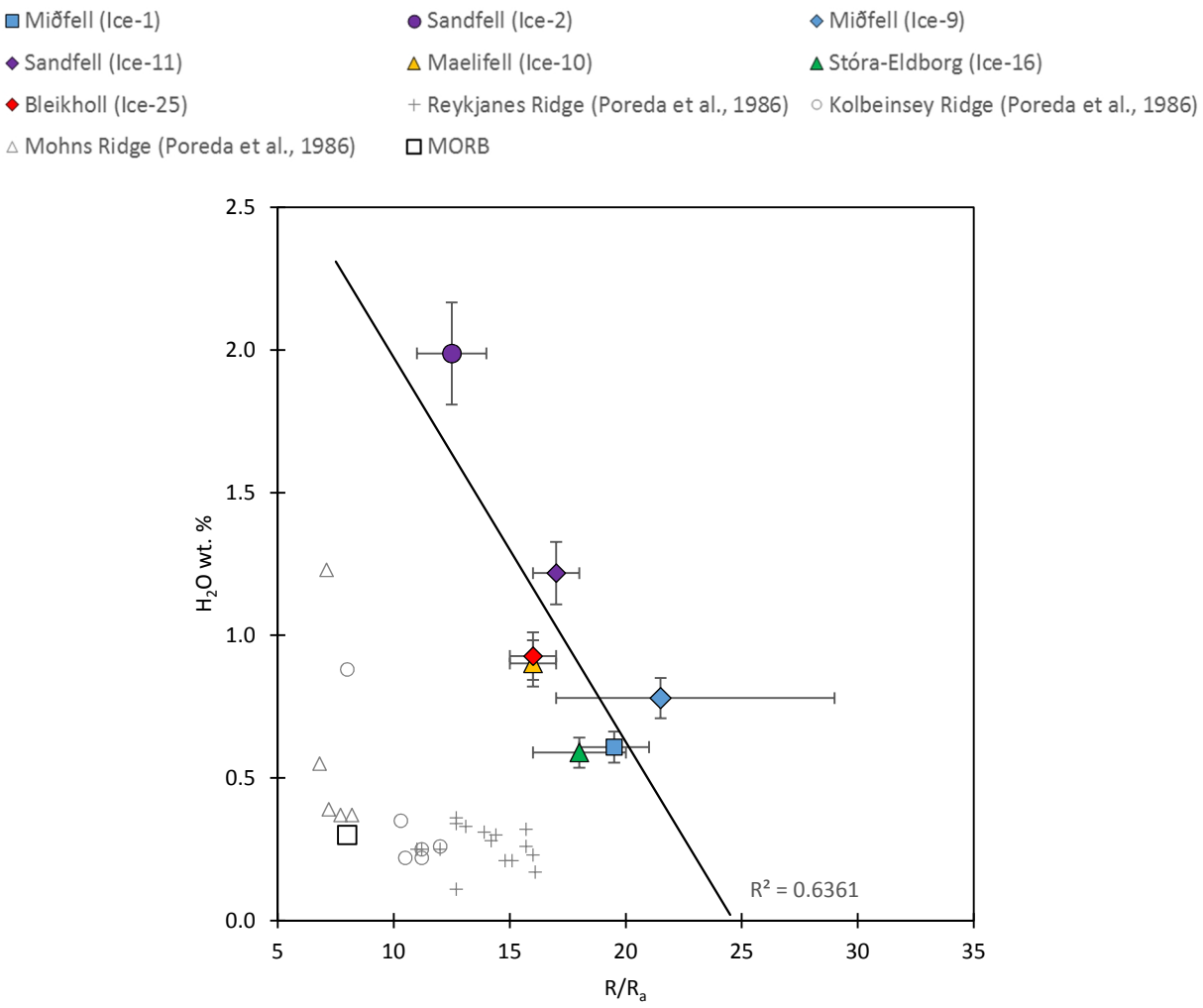

Figure 11: Maximum H_2O concentrations as a function of R/R_a for the melt inclusion analyzed in this study. For Ice-1, Ice-2 and Ice-9, the mean R/R_a values were used and the X-error bars represent the range of R/R_a values reported by Dixon et al. (2000) and Dixon (2003). For Ice-10, Ice-11, Ice-16 and Ice-25, 1σ error bars are shown from Dixon et al. (2000) and Dixon (2003). Y-error bars represent the maximum 2σ error for H_2O measurements over all analyses. Data from Poreda et al. (1986) are included for comparison along with the average MORB composition (Graham, 2002; Danyushevsky, 2001).

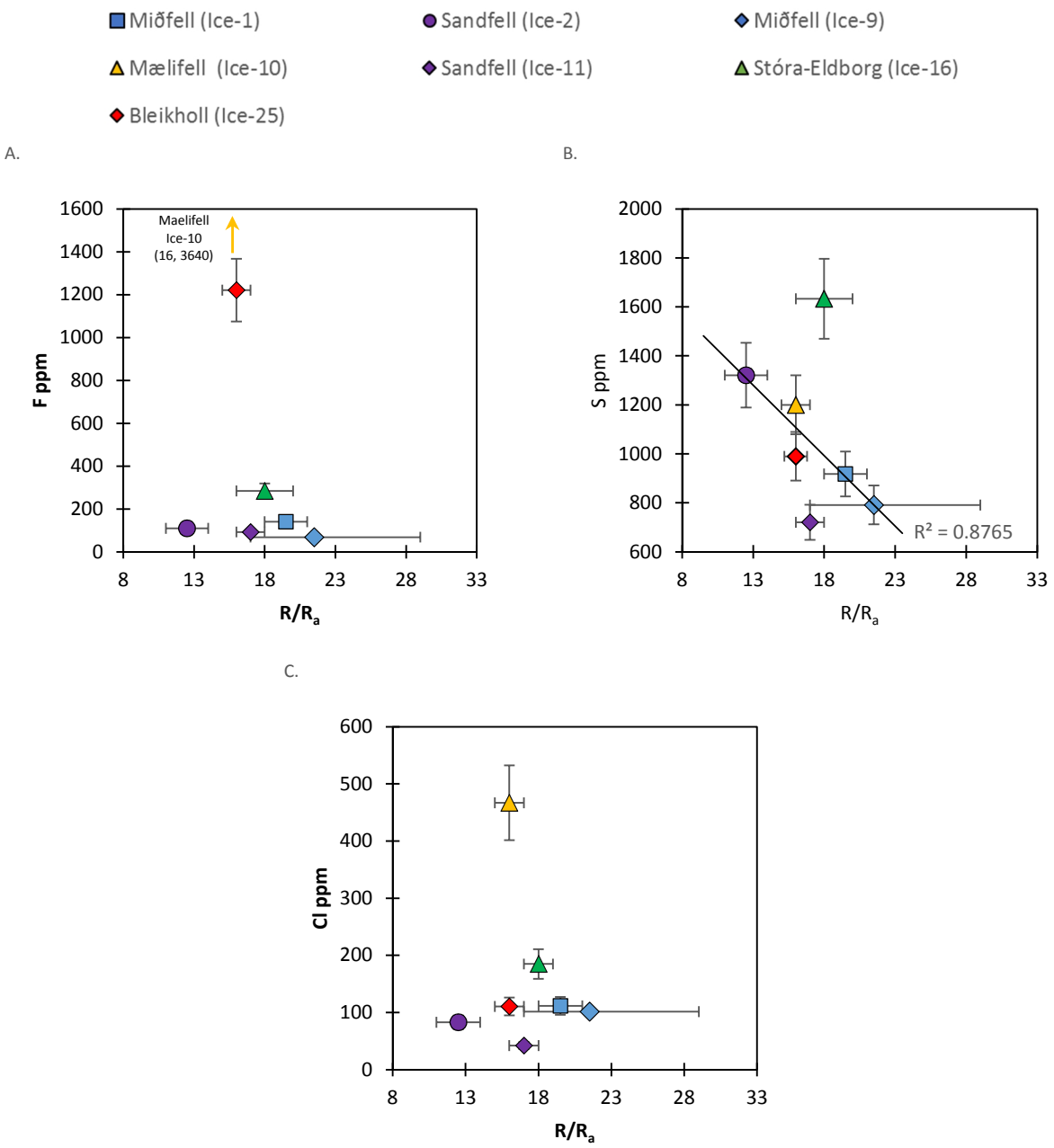

Figure 12: Maximum volatile compositions as a function of R/R_a for the melt inclusion analyzed in this study. For Ice-1, Ice-2 and Ice-9, the mean R/R_a values were used and the X-error bars represent the range of R/R_a values reported by Dixon et al. (2000) and Dixon (2003). For Ice-10, Ice-11, Ice-16 and Ice-25, 1σ error bars are shown from Dixon et al. (2000) and Dixon (2003). Y-error bars represent the maximum 2σ error for the respective volatile species over all analyses. The regression line in (B) does not include the Sandfell and Stóra-Eldborg data points, see text for discussion.

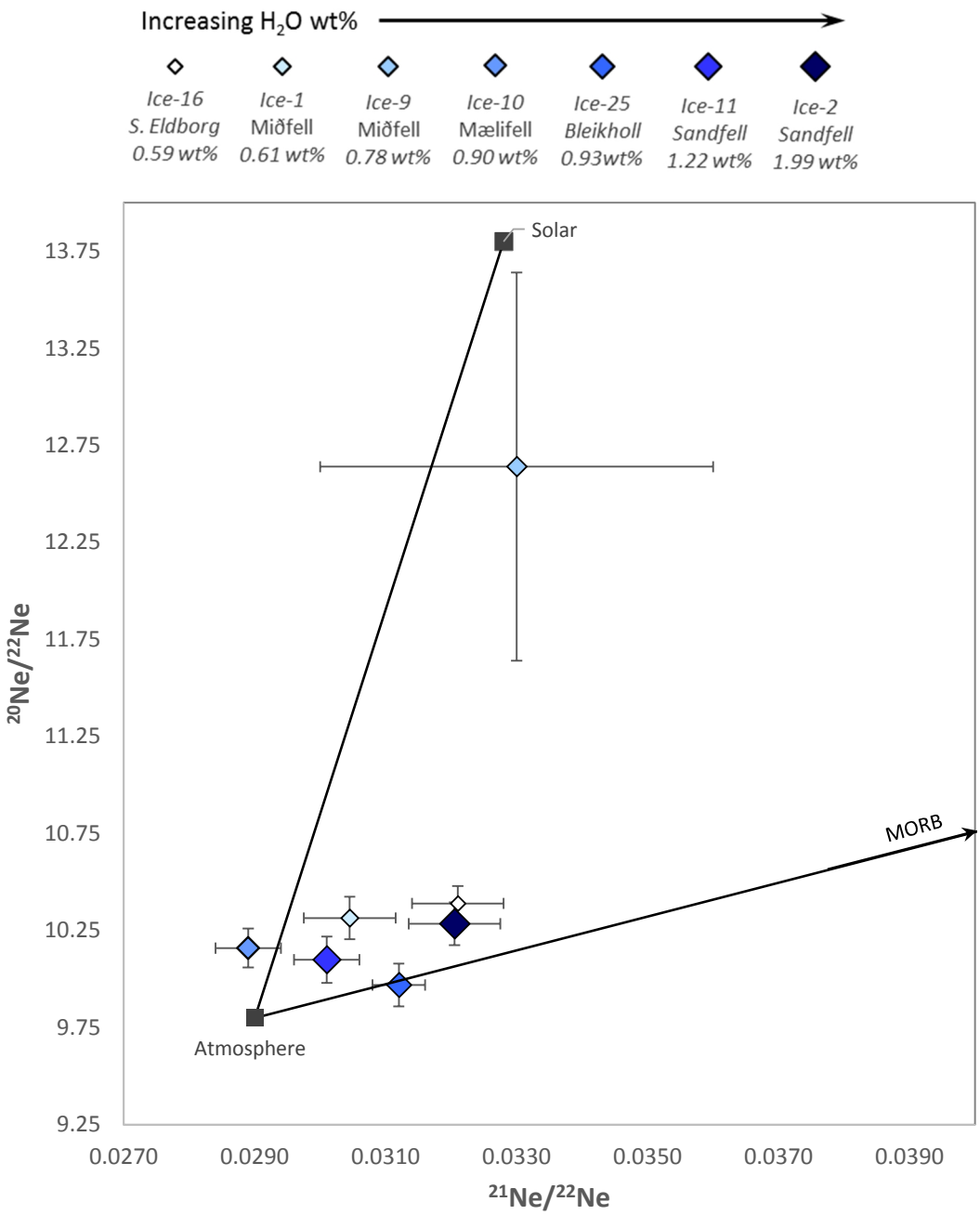

Figure 13: Three neon plot for the Reykjanes Peninsula samples. Neon data from Dixon et al. (2000) and Dixon (2003), replicate analyses were averaged for this study, 1 σ uncertainties are shown. Symbol size and color indicate H_2O concentrations in melt inclusions. Measured H_2O concentrations are shown in the legend. Atmosphere-MORB mixing line is from Moreira et al. (1998), and the solar end member is from Mahaffy (1998) and Pepin et al. (1999).

5.4 Origin of Volatiles in the Iceland Plume

5.4.1 Binary Mixing and Melt Extraction

Several studies have attributed the apparent decoupling of He-Ne in Icelandic lavas to binary mixing between a plume and MORB end member (Moreira et al., 2001; Dixon, 2003; Furi et al., 2010). The binary mixing model is complicated because the plume component with high $^{3}He/^{4}He$, and relative depletions in Ne (a reduction in Ne concentrations and loss of solar-like Ne isotopic compositions), mixes with the depleted/degassed MORB mantle, and subsequently undergoes degassing at shallow levels (Furi et al., 2010). A binary mixing model between a MORB component and a plume component can be invoked to explain the relationship between the variations in H_2O and noble gas signatures.

As suggested above (Section 5.2) the melting of two unique mantle lithologies can be inferred by comparing the water concentrations to the pressure of melt extraction as predicted by the barometric model in (Lee et al., 2009). The melting of a peridotite–pyroxenite mantle to produce the observed Icelandic magmas has been inferred in recent studies (Shorttle and Maclennan 2011; Koornneef et al., 2012). The observed relationship between H_2O and Ne isotopes may be the result of melting and mixing of enriched and depleted mantle domains as described above.

Water concentrations in the Stora-Eldborg, Bleikholl, and Sandfell samples all correlate with the depth of melt extraction and plot along a single well-defined trend in Figure 10. Furthermore, the Stora-Eldborg, Bleikholl, and Sandfell samples all plot along the atmosphere – MORB mixing line on a Ne isotope plot (Figure 13). Conversely, the Miðfell samples, which diverge from the trend in Figure 10, plot along the atmosphere – solar mixing line on the three Ne

isotope plot (Figure 13). This relationship may suggest that the presumed peridotite lithology responsible for the Miðfell magmas contains a solar Ne and primitive He component that is lacking in the hypothesized pyroxenite source.

With increasing source enrichment (i.e., high Nb/Zr or La/Sm), H_2O/K_2O values typically decrease (Michael, 1995). Water concentrations from the Reykjanes Peninsula melt inclusions studied here, decrease with decreasing H_2O/K_2O (e.g., Figure 5.H). While the low K_2O concentrations reported in this study are not well constrained given the large uncertainties in the measurements, qualitatively the H_2O/K_2O values generally decrease with increasing R/R_a. For example, the Miðfell sample Ice-9, has the highest R/R_a used in this study (mean R/R_a= 21.5, maximum R/R_a= 29) and the second lowest H_2O/K_2O (= 3.7). The relationship between H_2O/K_2O and R/R_a for the samples studied here suggests that samples showing higher R/R_a and lower H_2O/K_2O values are enriched, and possibly represent comingled ancient recycled oceanic lithosphere and less differentiated mantle domains. A similar argument was invoked by Brandon et al. (2007) to describe the relationship between Os and noble gas isotopes.

If a binary mixing model between a recycled enriched plume component and MORB component is the case, it would follow that the H_2O from the enriched source is mixed with the more depleted MORB mantle. As increased fractionation and melt extraction occur, the combined processes, could give rise to the higher H_2O/K_2O and higher H_2O concentrations at lower R/R_a. Assimilation of hydrothermally altered crust into the magma chamber beneath Iceland could also be a means for enriching H_2O relative to K_2O (e.g., Sobolev et al., 1996; Dixon et al., 2002) and generating the high H_2O/K_2O observed for the studied melt inclusions. If assimilation of hydrothermally altered crust into the magma chamber was the source of enrichment, Cl concentrations in the melt inclusions should be more elevated as is the case in Loihi magmas

(Dixon and Clague 2001). Assimilation of a Cl-rich phase in Loihi lavas results in Cl concentrations reaching values as high as 2380 ppm in melt inclusions (Dixon and Clague 2001). Given the low Cl concentrations of the studied melt inclusion, assimilation of recently hydrothermally altered crust is unlikely. In general, the binary mixing model for H_2O heterogeneity in the plume and MORB components is in agreement with the plume-MORB binary mixing model that gives rise to the decoupling of He and Ne as suggested by Dixon (2003) and Furi et al. (2010).

5.4.2 Three Component Mixing

An alternative explanation is that the Iceland plume contains two unique plume components, a primitive component and one originating from ancient recycled crust, mixing with depleted MORB. Three-component mixing was applied to the Shona Ridge group and Discovery Ridge by Dixon et al. (2002), a region in the Southern Ocean that shows solar Ne and primordial $^3He/^4He$ coupled with evidence of a recycled plume component. The authors showed that the Depleted MORB Mantle (DMM) component for Shona Group 1 has H_2O/K_2O = ~5 and H_2O/Ce =150 ± 10, and the FOZO component has H_2O/K_2O = ~0.8 and H_2O/Ce =210 ± 30 (Dixon et al., 2002). The ancient recycled enriched mantle (EM) component in the Discovery plume had lower H_2O coupled with lower H_2O/Ce, H_2O = ~0.5 wt. % and H_2O/Ce = ~150. They established that the HIMU mantle component, as determined from measurements of eclogite, has H_2O ~600 ppm, whereas the FOZO component is predicted to contain ~750 ppm. Dixon et al. (2002) concluded that plumes originating from recycled material are "damp" while plumes originating from FOZO are "wet."

Several of the H_2O/K_2O values for the Reykjanes Peninsula melt inclusions studied here are similar to the depleted MORB component from the Shona Ridge and Easter-Salas y Gomaz seamounts, both having H_2O/K_2O = ~5 (cf. Dixon et al., 2002), or in the case of Iceland with

several values from this study exceeding 5. Conversely, Nichols et al. (2002) reported several low H_2O/K_2O (<1); these low values are similar to the common plume component of the Shona Ridge group in the Southern Ocean (Dixon et al., 2002). Michael (1995) demonstrated that Northern MAR, including samples from Iceland, have high mean H_2O/Ce ~280±37, values more representative of the common, less degassed, mantle component suggested by Dixon et al. (2002). The mantle-source H_2O concentration beneath Iceland proposed by Nichols et al. (2002) ranges from 620 to 920 ppm, and the H_2O concentrations for the melt inclusions presented here confirm this estimate. The lower approximation for H_2O in the Iceland mantle, 620 ppm, is in general agreement with the HIMU estimates of Dixon et al. (2002). However, the values for mantle H_2O in the plume beneath Iceland reported by Nichols et al. (2002) span the range of both the HIMU and FOZO H_2O estimates proposed by Dixon et al. (2002).

As demonstrated above, the new data presented here in concert with previously reported data for Iceland and the Northern Atlantic (e.g., Poreda et al., 1986; Michael, 1995; Nichols et al., 2002) encompass the three-end-member magma-source components proposed by Dixon et al. (2002). However, the recycled plume component beneath Iceland appears enriched in volatiles relative to the common plume component and MORB. A volatile-enriched, recycled plume component is suggested by the relationship between enrichments in H_2O concentration with decreasing R/R_a (Figure 11), coupled with the observation that two of the three lowest H_2O concentrations reported here plot close to the atmosphere – solar mixing line on a three Ne plot (Figure 13). Further arguments supporting the presence of a volatile-enriched, recycled plume component beneath Iceland include the observation that the highest H_2O concentrations plot on the atmosphere – MORB mixing line.

Three-component mixing between a less degassed mantle component with high $^{3}He/^{4}He$ and low H_2O, a recycled mantle component with low $^{3}He/^{4}He$ and high H_2O, and depleted MORB, was invoked to describe the relationship between $^{3}He/^{4}He$ and H_2O in the region encompassing the Reykjanes, Kolbleinsy, and Mohns Ridges by Poreda et al. (1986). The melt inclusions studied here follow a similar pattern to, but are unique from, the data for the individual ridge segments reported in Poreda et al. (1986) (Figure 11). Michael (1995) applied the three-component mixing model to the Reykjanes Ridge, and argued for rapid subduction as the source of high H_2O/Ce and the origin of recycled material, including volatiles into the Northern Atlantic mantle.

5.4.3 Conceptual Model for the Source of Ancient Recycled Crust

Both the binary mixing model between a pyroxenite-peridotite mantle and three-component mixing model, require ancient recycled lithosphere incorporated into the mantle. Several workers have proposed recycled, subducted, material beneath Iceland on the basis of radiogenic isotopes and trace elements (e.g., Chauvel and Hemond, 2000; Skovgaard et al., 2001; Breddam, 2002; Stracke et al., 2003a; 2003b; Kokfelt et al., 2006; Brandon et al., 2007; Sobolev et al., 2008). While a HIMU-like component was suggested as a source for the enriched alkaline rocks on Iceland (Stracke et al., 2003a; Kokfelt et al., 2006), the picrites are believed to originate from a depleted plume component completely dissimilar to HIMU (Kokfelt et al., 2006). Both the HIMU-like and depleted components were proposed to originate from the subduction of an entire section of oceanic crust, the HIMU-like component deriving from the upper hydrothermally altered crust, and the depleted component resulting from the gabbroic and ultramafic cumulates (Kokfelt et al., 2006). Kokfelt et al. (2006) inferred using Pb isotope data that the average age of recycled crust beneath Iceland is ~1.5 Ga. Additionally, Sobolev et al. (2008) demonstrated that the correlation between $^{187}Os/^{188}Os$, Mn and Ni, can be modeled as 1.1-1.8-Ga recycled oceanic crust

reacted with peridotite. A study of Os and He isotopes in Iceland showed that the relationship between $^{187}Os/^{188}Os$ and $^{3}He/^{4}He$ coupled with solar Ne, is consistent with ~1-1.5 Ga recycled lithosphere being mixed with primitive, high $^{3}He/^{4}He$, mantle near the core-mantle boundary (Brandon et al., 2007).

Seismic studies have demonstrated a possible lower mantle origin for the Iceland plume (Helmberger et al., 1998; Bijwaard and Spakman, 1999), but this observation is debated as other geophysical methods place the plume at shallower mantle depths of no more than the 670-km discontinuity (e.g., Wolfe et al. 1997; Ritsema and Allen 2003). Regardless of the depth of the plume, Shaw et al. (2012) suggested from their investigation of Manus Basin volcanic glasses, that water and H isotope anomalies are potentially transferred to the deep mantle via subduction, and are preserved for up to 10^9 years.

The mantle plume beneath Iceland was located north of Greenland at approximately 130 Ma and migrated to its present day location as the North American Plate moved westward (Figure 14; L. Lawver, UTIG, personal communication). A conceptual model for the origin of volatiles in the North Atlantic mantle as a consequence of subduction beneath Greenland during the Paleoproterozoic Ketilidian Orogeny is presented in Figure 15. During the Paleoproterzoic Ketilidian Orogeny, ca. 1850 – 1720 Ma, (Garde et al., 2002) an oceanic plate was subducted beneath the current southern margin of Greenland as oblique convergence between Greenland and an oceanic plate occurred (Chadwick and Garde 1996; Garde et al., 2002). The age of subduction beneath Greenland presented in Garde et al., (2002) is in general agreement with the range of ages (1-1.8 Ga) presented by Kokfelt et al. (2006), Brandon et al. (2007), and Sobolev et al. (2008) for the age of recycled material incorporated into the plume beneath Iceland. If subduction during the

Ketilidian Orogeny was rapid this could have supplied volatiles to the mantle resulting in the high H_2O/Ce reported by Michael (1995).

In the conceptual model, hydrothermally altered oceanic material is subducted into the mantle beneath Greenland. During subduction He is volatilized, removing both ^{3}He and ^{4}He, the remaining He concentration is subjected to the time integrated alpha decay of Th and U to produce ^{4}He relative to ^{3}He, thereby lowering the R/R_a ratio of the subducted material (Poreda et al., 1986). Given the proposed oblique angle of convergence (Garde et al., 2002), it is possible that horizontal propagating tears in the subducted plate removed sections of down-going slab and isolated hydrothermally altered, volatile enriched, sections of slab within the less differentiated mantle. The foundering and subsequent melting of the volatile-rich, hydrothermally altered oceanic material results in the juxtaposition of recycled slab signatures against less differentiated mantle domains as proposed by Brandon et al. (2007). The culmination of these events causes volatile enrichment in the mantle and leads to the observed heterogeneous isotopic and trace element composition of the plume (e.g., Poreda et al., 1986; Michael 1995; Chauvel and Hemond, 2000; Skovgaard et al., 2001; Breddam, 2002; Stracke et al., 2003a; 2003b; Kokfelt et al., 2006; Brandon et al., 2007; Sobolev et al., 2008).

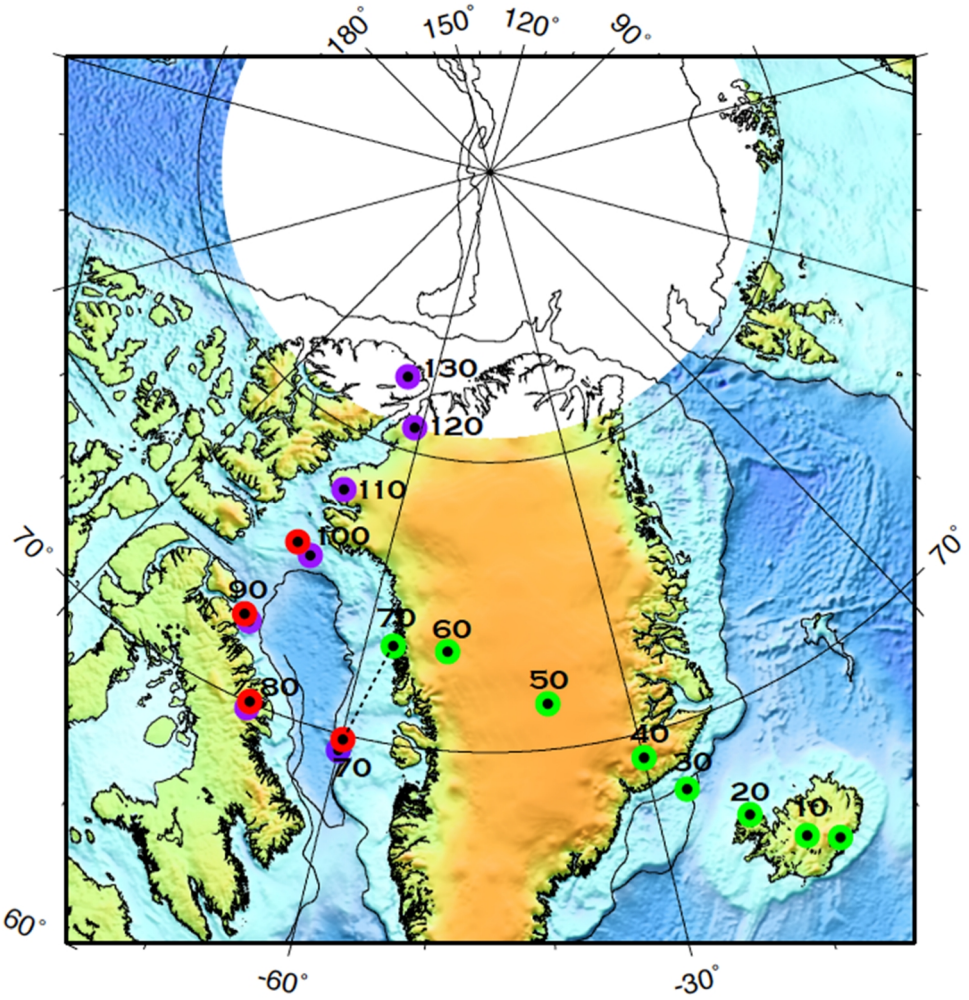

Figure 14: Map of the Northern Atlantic showing paleotectonic models representing the trace of the Iceland Plume from 130 Ma to present. Purple dots represent the migration of the plume between 130 – 70 Ma assuming a tectonically fixed position for the North Americon Massif. Red dots indicate the trace of the plume between 100 Ma – 70 Ma assuming a tectonically fixed position for Baffin Island. The green dots indicate the trace of the plume from 70 Ma to present assuming a tectonically fixed position for Greenland. Figure courtesy of L. Lawver, UTIG, personal communication.

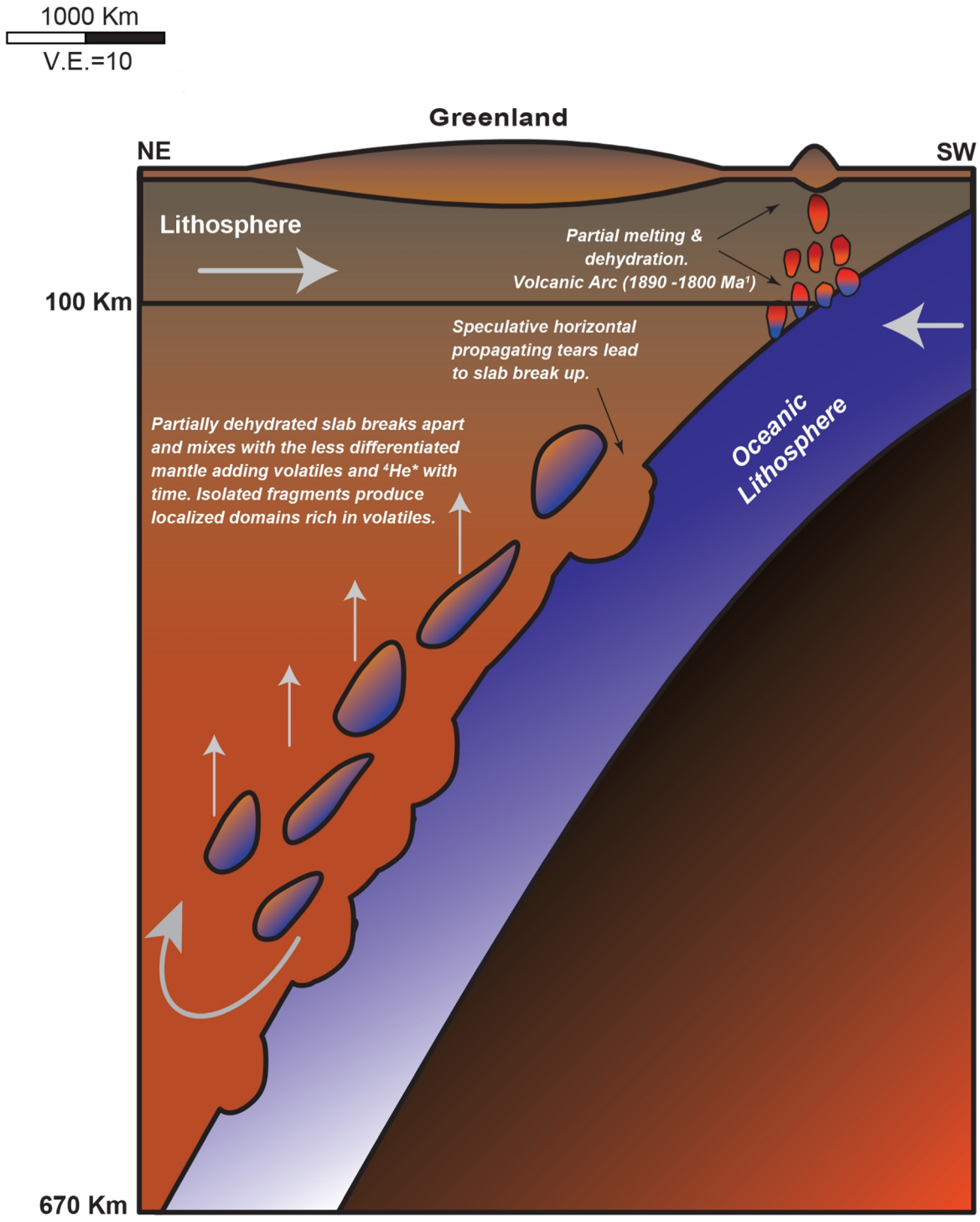

Figure 15: Conceptual model showing a possible origin of volatiles in the Iceland plume as a result of subduction. Subduction of oceanic lithosphere off the southern margin of Greenland during the Paleoproterozoic Ketilidian Orogeny (Garde et al., 2002). Speculative slab tears and foundering of the subducted slab leads to mixing of volatile rich recycled oceanic lithosphere with less differentiated mantle material. By 130 Ma it is possible that slab is melted and incorporated into the mantle, mantle plume migrates to present day location, see text for discussion. [1] Garde et al. 2002.

6. CONCLUSIONS AND FUTURE WORK

This study demonstrates that magmas from Iceland are enriched in volatiles. These findings in concert with data from the literature suggest that the mantle plume beneath Iceland contains a volatile-rich, recycled component with R/R_a values greater than those of MORB, and yet with MORB-like Ne isotopic ratios, as well as a volatile-poor, plume component with high R/R_a and solar Ne. The conceptual model presented in this study shows a possible means for the incorporation of hydrothermally altered oceanic lithosphere during the Ketilidian Orogoney (1850 – 1720 Ma) beneath Greenland and corroborates the age of recycled oceanic lithosphere in the mantle beneath Iceland presented by Kokfelt et al. (2006), Brandon et al. (2007), and Sobolev et al. (2008). In order to further understand the origin of volatiles in the Iceland plume, a survey of trace elements, including H_2O/Ce, on the melt inclusions studied here, must be conducted and related to the source rock isotopic compositions. The major conclusions may be summarized as follows:

1. Major-oxide concentration in the melt inclusions from the Reykjanes Peninsula are less differentiated than the basaltic glasses from the Hengíll Swarm studied by Tronnes (1990). The melt inclusion compositions are related to the Hengíll Swarm basaltic glass by the progressive crystallization and fractionation of olivine and plagioclase.
2. Volatile concentrations in melt inclusions are heterogeneous for all species (CO_2, H_2O, F, S, and Cl) throughout the Reykjanes Peninsula and no relationship exists between the volatile and major-oxide concentrations.

3. The maximum measured H_2O concentrations on olivine-hosted inclusions in the Icelandic suite of samples previously analyzed for He and Ne isotopic by Dixon et al. (2000) and Dixon (2003) is 1.99 ± 0.06 wt. %. The range of H_2O abundances are in agreement with values reported for basaltic glass by Nichols et al. (2002), and likely represent minimum concentrations because of the evidence for degassing.
4. Besides H_2O, melt inclusions have also lost significant amounts of CO_2, S, and Cl. Calculations of entrapment-pressure based on the vapor saturation of CO_2 and H_2O yield values from <10 to 300 MPa. Degassing occurred at low pressure and concurrently with crystallization.
5. Volatile concentrations decrease with increasing R/R_a, and the highest H_2O concentrations plot along the atmosphere-MORB mixing line in three-neon-isotope space. Two of the three lowest H_2O concentrations measured plot along the solar-atmosphere mixing line. These findings suggest that a volatile-enriched recycled component with high H_2O and low $^3He/^4He$ values has mixed with a primitive mantle component that is low in H_2O but has high $^3He/^4He$ values.

REFERENCES

Asimow, P.D., Hirschmann, M.M., and Stolper, E.M., 2001, Calculation of Peridotite Partial Melting from Thermodynamic Models of Minerals and Melts, IV. Adiabatic Decompression and the Composition and Mean Properties of Mid-ocean Ridge Basalts: Journal of Petrology, v. 42, p. 963–998.

Asimow, P.D., and Langmuir, C.H., 2003, The importance of water to oceanic mantle melting regimes: Nature, v. 421, p. 815–820.

Bijwaard, H., and Spakman, W., 1999, Tomographic evidence for a narrow whole mantle plume below Iceland: Earth and Planetary Science Letters, v. 166, p. 121–126.

Brandon, A.D., Graham, D.W., Waight, T., and Gautason, B., 2007, ^{186}Os and ^{187}Os enrichments and high-$^{3}He/^{4}He$ sources in the Earth's mantle: Evidence from Icelandic picrites: Geochimica et Cosmochimica Acta, v. 71, p. 4570–4591.

Breddam, K., 2002, Kistufell: Primitive Melt from the Iceland Mantle Plume: Journal of Petrology, v. 43, p. 345–373.

Bucholz, C.E., Gaetani, G.A., Behn, M.D., and Shimizu, N., 2013, Post-entrapment modification of volatiles and oxygen fugacity in olivine-hosted melt inclusions: Earth and Planetary Science Letters, v. 374, p. 145–155.

Cabato, J.A., Stefano, C.J., and Mukasa, S.B., 2015, Volatile concentrations in olivine-hosted melt inclusions from the Columbia River flood basalts and associated lavas of the Oregon Plateau: Implications for magma genesis: Chemical Geology, v. 392, p. 59–73.

Chadwick, B., and Garde, A.A., 1996, Palaeoproterozoic oblique plate convergence in South Greenland: a reappraisal of the Ketilidian Orogen: Geological Society, London, Special Publications, v. 112, p. 179–196.

Chauvel, C., and Hémond, C., 2000, Melting of a complete section of recycled oceanic crust: Trace element and Pb isotopic evidence from Iceland: Geochemistry, Geophysics, Geosystems, v. 1, 1999GC000002.

Danyushevsky, L.V., Della-Pasqua, F.N., and Sokolov, S., 2000, Re-equilibration of melt inclusions trapped by magnesian olivine phenocrysts from subduction-related magmas: petrological implications: Contributions to Mineralogy and Petrology, v. 138, p. 68–83.

Danyushevsky, L.V., 2001, The effect of small amounts of H_2O on crystallisation of mid-ocean ridge and backarc basin magmas: Journal of Volcanology and Geothermal Research, v. 110, p. 265–280.

Danyushevsky, L.V., McNeill, A.W., and Sobolev, A.V., 2002, Experimental and petrological studies of melt inclusions in phenocrysts from mantle-derived magmas: an overview of techniques, advantages and complications: Chemical Geology, v. 183, p. 5–24.

Darbyshire, F.A., Priestley, K.F., White, R.S., Stefánsson, R., Gudmundsson, G.B., and Jakobsdóttir, S.S., 2000, Crustal structure of central and northern Iceland from analysis of teleseismic receiver functions: Geophysical Journal International, v. 143, p. 163–184.

Davis, A.S., Clague, D.A., Schulz, M.S., and Hein, J.R., 1991, Low sulfur content in submarine lavas: An unreliable indicator of subaerial eruption: Geology, v. 19, p. 750–753.

Dixon, E.T., Honda, M., McDougall, I., Campbell, I.H., and Sigurdsson, I., 2000, Preservation of near-solar neon isotopic ratios in Icelandic basalts: Earth and Planetary Science Letters, v. 180, p. 309–324.

Dixon, E.T., 2003, Interpretation of helium and neon isotopic heterogeneity in Icelandic basalts: Earth and Planetary Science Letters, v. 206, p. 83–99.

Dixon, J.E., and Clague, D.A., 2001, Volatiles in Basaltic Glasses from Loihi Seamount, Hawaii: Evidence for a Relatively Dry Plume Component: Journal of Petrology, v. 42, p. 627–654.

Dixon, J.E., Clague, D.A., and Stolper, E.M., 1991, Degassing History of Water, Sulfur, and Carbon in Submarine Lavas from Kilauea Volcano, Hawaii: The Journal of Geology, v. 99, p. 371–394.

Dixon, J.E., Clague, D.A., Wallace, P., and Poreda, R., 1997, Volatiles in Alkalic Basalts form the North Arch Volcanic Field, Hawaii: Extensive Degassing of Deep Submarine-erupted Alkalic Series Lavas: Journal of Petrology, v. 38, p. 911–939.

Dixon, J.E., Leist, L., Langmuir, C., and Schilling, J.-G., 2002, Recycled dehydrated lithosphere observed in plume-influenced mid-ocean-ridge basalt: Nature, v. 420, p. 385–389.

Einarsson, A., 2012, Origin of macrocrysts and gabbro-nodules in Hengíll, SW Iceland: M.S. thesis, University of Iceland.

Ferk, A., and Leonhardt, R., 2009, The Laschamp geomagnetic field excursion recorded in Icelandic lavas: Physics of the Earth and Planetary Interiors, v. 177, p. 19–30.

Füri, E., Hilton, D.R., Halldórsson, S.A., Barry, P.H., Hahm, D., Fischer, T.P., and Grönvold, K., 2010, Apparent decoupling of the He and Ne isotope systematics of the Icelandic mantle: The role of He depletion, melt mixing, degassing fractionation and air interaction: Geochimica et Cosmochimica Acta, v. 74, p. 3307–3332.

Gaetani, G.A., and Grove, T.L., 1998, The influence of water on melting of mantle peridotite: Contributions to Mineralogy and Petrology, v. 131, p. 323–346.

Garde, A.A., Hamilton, M.A., Chadwick, B., Grocott, J., and McCaffrey, K.J.W., 2002, The Ketilidian orogen of South Greenland: geochronology, tectonics, magmatism, and fore-arc accretion during Palaeoproterozoic oblique convergence: Canadian Journal of Earth Sciences, v. 39, p. 765–793.

Geirsdóttir, Á., Miller, G.H., Axford, Y., and Ólafsdóttir, S., 2009, Holocene and latest Pleistocene climate and glacier fluctuations in Iceland: Quaternary Science Reviews, v. 28, p. 2107–2118.

Ghiorso, M.S., and Sack, R.O., 1995, Chemical mass transfer in magmatic processes IV. A revised and internally consistent thermodynamic model for the interpolation and extrapolation of liquid-solid equilibria in magmatic systems at elevated temperatures and pressures: Contributions to Mineralogy and Petrology, v. 119, p. 197–212.

Graham, D.W., 2002, Noble Gas Isotope Geochemistry of Mid-Ocean Ridge and Ocean Island Basalts: Characterization of Mantle Source Reservoirs: Reviews in Mineralogy and Geochemistry, v. 47, p. 247–317.

Gurenko, A., and Sobolev, A., 2006, Crust–primitive magma interaction beneath neovolcanic rift zone of Iceland recorded in gabbro xenoliths from Miðfell, SW Iceland: Contributions to Mineralogy and Petrology, v. 151, p. 495–520.

Harrison, D., Burnard, P., and Turner, G., 1999, Noble gas behaviour and composition in the mantle: constraints from the Iceland Plume: Earth and Planetary Science Letters, v. 171, p. 199–207.

Hauri, E., Wang, J., Dixon, J.E., King, P.L., Mandeville, C., and Newman, S., 2002, SIMS analysis of volatiles in silicate glasses: 1. Calibration, matrix effects and comparisons with FTIR: Chemical Geology, v. 183, p. 99–114.

Helmberger, D.V., Wen, L., and Ding, X., 1998, Seismic evidence that the source of the Iceland hotspot lies at the core–mantle boundary: Nature, v. 396, p. 251–255.

Helo, C., Longpré, M.-A., Shimizu, N., Clague, D.A., and Stix, J., 2011, Explosive eruptions at mid-ocean ridges driven by CO_2-rich magmas: Nature Geoscience, v. 4, p. 260–263.

Hilton, D.R., Thirlwall, M.F., Taylor, R.N., Murton, B.J., and Nichols, A., 2000, Controls on magmatic degassing along the Reykjanes Ridge with implications for the helium paradox: Earth and Planetary Science Letters, v. 183, p. 43–50.

Hirose, K., and Kawamoto, T., 1995, Hydrous partial melting of lherzolite at 1 GPa: The effect of H_2O on the genesis of basaltic magmas: Earth and Planetary Science Letters, v. 133, p. 463–473.

Hirschmann, M.M., Kogiso, T., Baker, M.B., and Stolper, E.M., 2003, Alkalic magmas generated by partial melting of garnet pyroxenite: Geology, v. 31, p. 481–484.

Ingólfsson, Ó., Björck, S., Haflidason, H., and Rundgren, M., 1997, Glacial and climatic events in Iceland reflecting regional North Atlantic climatic shifts during the Pleistocene-Holocene transition: Quaternary Science Reviews, v. 16, p. 1135–1144.

Hofmann, A.W., and White, W.M., 1982, Mantle plumes from ancient oceanic crust: Earth and Planetary Science Letters, v. 57, p. 421–436.

Jakobsson, S.P., and Johnson, G.L., 2012, Intraglacial volcanism in the Western Volcanic Zone, Iceland: Bulletin of Volcanology, v. 74, p. 1141–1160.

Jakobsson, S.P., Jónsson, J., and Shido, F., 1978, Petrology of the Western Reykjanes Peninsula, Iceland: Journal of Petrology, v. 19, p. 669–705.

Jambon, A., and Zimmermann, J.L., 1990, Water in oceanic basalts: evidence for dehydration of recycled crust: Earth and Planetary Science Letters, v. 101, p. 323–331.

Jambon, A., Déruelle, B., Dreibus, G., and Pineau, F., 1995, Chlorine and bromine abundance in MORB: the contrasting behaviour of the Mid-Atlantic Ridge and East Pacific Rise and implications for chlorine geodynamic cycle: Chemical Geology, v. 126, p. 101–117.

Johnson, E.R., Wallace, P.J., Cashman, K.V., and Delgado Granados, H., 2010, Degassing of volatiles (H_2O, CO_2, S, Cl) during ascent, crystallization, and eruption at mafic monogenetic volcanoes in central Mexico: Journal of Volcanology and Geothermal Research, v. 197, p. 225–238.

Jull, M., and McKenzie, D., 1996, The effect of deglaciation on mantle melting beneath Iceland: Journal of Geophysical Research: Solid Earth, v. 101, p. 21815–21828.

Kokfelt, T.F., Hoernle, K., Hauff, F., Fiebig, J., Werner, R., and Garbe-Schönberg, D., 2006, Combined Trace Element and Pb-Nd–Sr-O Isotope Evidence for Recycled Oceanic Crust (Upper and Lower) in the Iceland Mantle Plume: Journal of Petrology, v. 47, p. 1705–1749.

Koornneef, J.M., Stracke, A., Bourdon, B., Meier, M.A., Jochum, K.P., Stoll, B., and Grönvold, K., 2012, Melting of a Two-component Source beneath Iceland: Journal of Petrology, v. 53, p. 127–157, doi: 10.1093/petrology/egr059.

Kushiro, I., Syono, Y., and Akimoto, S., 1968, Melting of a peridotite nodule at high pressures and high water pressures: Journal of Geophysical Research, v. 73, p. 6023–6029.

Lee, C.-T.A., Luffi, P., Plank, T., Dalton, H., and Leeman, W.P., 2009, Constraints on the depths and temperatures of basaltic magma generation on Earth and other terrestrial planets using new thermobarometers for mafic magmas: Earth and Planetary Science Letters, v. 279, p. 20–33.

Licciardi, J.M., Kurz, M.D., and Curtice, J.M., 2006, Cosmogenic ^{3}He production rates from Holocene lava flows in Iceland: Earth and Planetary Science Letters, v. 246, p. 251–264.

Licciardi, J.M., Kurz, M.D., and Curtice, J.M., 2007, Glacial and volcanic history of Icelandic table mountains from cosmogenic ^{3}He exposure ages: Quaternary Science Reviews, v. 26, p. 1529–1546.

Licciardi, J.M., Denoncourt, C.L., and Finkel, R.C., 2008, Cosmogenic ^{36}Cl production rates from Ca spallation in Iceland: Earth and Planetary Science Letters, v. 267, p. 365–377.

Maclennan, J., Jull, M., McKenzie, D., Slater, L., and Grönvold, K., 2002, The link between volcanism and deglaciation in Iceland: Geochemistry, Geophysics, Geosystems, v. 3, p. 1062.

Mathews, W.H., 1947, "Tuyas," flat-topped volcanoes in northern British Columbia: American Journal of Science, v. 245, p. 560–570.

Mathez, E.A., 1976, Sulfur solubility and magmatic sulfides in submarine basalt glass: Journal of Geophysical Research, v. 81, p. 4269–4276.

Mahaffy, P.R., Donahue, T.M., Atreya, S.K., Owen, T.C., and Niemann, H.B., 1998, Galileo Probe Measurements of D/H and 3He/4He in Jupiter's Atmosphere: Space Science Reviews, v. 84, p. 251–263.

McKenzie, D., 1985, The extraction of magma from the crust and mantle: Earth and Planetary Science Letters, v. 74, p. 81–91.

Métrich, N., Sigurdsson, H., Meyer, P.S., and Devine, J.D., 1991, The 1783 Lakagigar eruption in Iceland: geochemistry, CO_2 and sulfur degassing: Contributions to Mineralogy and Petrology, v. 107, p. 435–447.

Métrich, N., and Wallace, P.J., 2008, Volatile Abundances in Basaltic Magmas and Their Degassing Paths Tracked by Melt Inclusions: Reviews in Mineralogy and Geochemistry, v. 69, p. 363–402.

Métrich, N., Zanon, V., Créon, L., Hildenbrand, A., Moreira, M., and Marques, F.O., 2014, Is the "Azores Hotspot" a Wetspot? Insights from the Geochemistry of Fluid and Melt Inclusions in Olivine of Pico Basalts: Journal of Petrology, v. 55, p. 377–393.

Michael, P., 1995, Regionally distinctive sources of depleted MORB: Evidence from trace elements and H2O: Earth and Planetary Science Letters, v. 131, p. 301–320.

Michael, P.J., and Cornell, W.C., 1998, Influence of spreading rate and magma supply on crystallization and assimilation beneath mid-ocean ridges: Evidence from chlorine and major element chemistry of mid-ocean ridge basalts: Journal of Geophysical Research: Solid Earth, v. 103.

Michael, P.J., and Schilling, J.-G., 1989, Chlorine in mid-ocean ridge magmas: Evidence for assimilation of seawater-influenced components: Geochimica et Cosmochimica Acta, v. 53, p. 3131–3143.

Moore, J.G., 1965, Petrology of deep sea basalt near Hawaii: American Journal of Science, v. 263, p. 40–52.

Moore, J.G., Clague, D.A., and Normark, W.R., 1982, Diverse basalt types from Loihi seamount, Hawaii: Geology, v. 10, p. 88–92.

Moreira, M., Breddam, K., Curtice, J., and Kurz, M.D., 2001, Solar neon in the Icelandic mantle: new evidence for an undegassed lower mantle: Earth and Planetary Science Letters, v. 185, p. 15–23.

Newman, S., and Lowenstern, J.B., 2002, VolatileCalc: a silicate melt–H_2O–CO_2 solution model written in Visual Basic for excel: Computers and Geosciences, v. 28, p. 597–604.

Nichols, A.R.L., Carroll, M.R., and Höskuldsson, Á., 2002, Is the Iceland hot spot also wet? Evidence from the water contents of undegassed submarine and subglacial pillow basalts: Earth and Planetary Science Letters, v. 202, p. 77–87.

Nielsen, R.L., Michael, P.J., and Sours-Page, R., 1998, Chemical and Physical Indicators of Compromised Melt Inclusions: Geochimica et Cosmochimica Acta, v. 62, p. 831–839.

Norðdahl, H., and Pétursson, H.G., 2005, 3. Relative sea-level changes in Iceland: new aspects of the Weichselian deglaciation of Iceland, *in* C. Caseldine, A.R., J. Harðardóttir and Ó. Knudsen ed., Developments in Quaternary Sciences, Iceland — Modern Processes and Past Environments, Elsevier, p. 25–78.

Peate, D.W., Baker, J.A., Jakobsson, S.P., Waight, T.E., Kent, A.J.R., Grassineau, N.V., and Skovgaard, A.C., 2009, Historic magmatism on the Reykjanes Peninsula, Iceland: a snap-shot of melt generation at a ridge segment: Contributions to Mineralogy and Petrology, v. 157, p. 359–382.

Pepin, R.O., Becker, R.H., and Schlutter, D.J., 1999, Irradiation records in regolith materials. I: isotopic compositions of solar-wind neon and argon in single lunar mineral grains: Geochimica et Cosmochimica Acta, v. 63, p. 2145–2162.

Poreda, R., Schilling, J.-G., and Craig, H., 1986, Helium and hydrogen isotopes in ocean-ridge basalts north and south of Iceland: Earth and Planetary Science Letters, v. 78, p. 1–17.

Risku-Norja, H., 1985, Gabbro nodules from a picritic pillow basalt, Miðfell, SW Iceland: NVI Research Report, 8601.

Robinson, C.J., Bickle, M.J., Minshull, T.A., White, R.S., and Nichols, A.R.L., 2001, Low degree melting under the Southwest Indian Ridge: the roles of mantle temperature, conductive cooling and wet melting: Earth and Planetary Science Letters, v. 188, p. 383–398.

Schilling, J.-G., 1973, Iceland Mantle Plume: Geochemical Study of Reykjanes Ridge: Nature, v. 242, p. 565–571.

Schilling, J.-G., Bergeron, M.B., Evans, R., and Smith, J.V., 1980, Halogens in the Mantle Beneath the North Atlantic: Philosophical Transactions of the Royal Society of London. Series A, Mathematical and Physical Sciences, v. 297, p. 147–178, doi.

Schilling, J.G., Zajac, M., Evans, R., Johnston, T., White, W., Devine, J.D., and Kingsley, R., 1983, Petrologic and geochemical variations along the Mid-Atlantic Ridge from 29 degrees N to 73 degrees N: American Journal of Science, v. 283, p. 510–586.

Shaw, A.M., Hauri, E.H., Behn, M.D., Hilton, D.R., Macpherson, C.G., and Sinton, J.M., 2012, Long-term preservation of slab signatures in the mantle inferred from hydrogen isotopes: Nature Geoscience, v. 5, p. 224–228.

Shorttle, O., and Maclennan, J., 2011, Compositional trends of Icelandic basalts: Implications for short–length scale lithological heterogeneity in mantle plumes: Geochemistry, Geophysics, Geosystems, v. 12, p. Q11008.

Sigmarsson, O., and Steinthórsson, S., 2007, Origin of Icelandic basalts: A review of their petrology and geochemistry: Journal of Geodynamics, v. 43, p. 87–100.

Sigvaldason, G.E., and Óskarsson, N., 1976, Chlorine in basalts from Iceland: Geochimica et Cosmochimica Acta, v. 40, p. 777–789.

Skovgaard, A.C., Storey, M., Baker, J., Blusztajn, J., and Hart, S.R., 2001, Osmium–oxygen isotopic evidence for a recycled and strongly depleted component in the Iceland mantle plume: Earth and Planetary Science Letters, v. 194, p. 259–275.

Sobolev, A.V., and Chaussidon, M., 1996, H_2O concentrations in primary melts from supra-subduction zones and mid-ocean ridges: Implications for H_2O Stórage and recycling in the mantle: Earth and Planetary Science Letters, v. 137, p. 45–55.

Sobolev, A.V., Hofmann, A.W., Brügmann, G., Batanova, V.G., and Kuzmin, D.V., 2008, A Quantitative Link Between Recycling and Osmium Isotopes: Science, v. 321, p. 536–536.

Stefano, C.J., Mukasa, S.B., Andronikov, A., and Leeman, W.P., 2010, Water and other volatile systematics of olivine-hosted melt inclusions from the Yellowstone hotspot track: Contributions to Mineralogy and Petrology, v. 161, p. 615–633.

Stracke, A., Zindler, A., Salters, V.J.M., McKenzie, D., and Grönvold, K., 2003b, The dynamics of melting beneath Theistareykir, northern Iceland: Geochemistry, Geophysics, Geosystems, v. 4, p. 8513.

Stracke, A., Zindler, A., Salters, V.J.M., McKenzie, D., Blichert-Toft, J., Albarède, F., and Grönvold, K., 2003a, Theistareykir revisited: Geochemistry, Geophysics, Geosystems, v. 4, p. 8507.

Trieloff, M., Kunz, J., Clague, D.A., Harrison, D., and Allègre, C.J., 2000, The Nature of Pristine Noble Gases in Mantle Plumes: Science, v. 288, p. 1036–1038.

Trønnes, R.G., 1990, Basaltic melt evolution of the Hengíll volcano system, SW Iceland, and evidence for clinopyroxene assimilation in primitive tholeiitic magmas: Journal of Geophysical Research, v. 95, p. 15,893–15,910.

Vargas, J.R., 1992, Geology and Geothermal Considerations of Krýsuvík Valley, Reykjanes Peninsula, Iceland: UNU Geothermal Training Programme 13, 35 p.

Wallace, P., and Carmichael, I.S.E., 1992, Sulfur in basaltic magmas: Geochimica et Cosmochimica Acta, v. 56, p. 1863–1874.

Wallace, P.J., 2005, Volatiles in subduction zone magmas: concentrations and fluxes based on melt inclusion and volcanic gas data: Journal of Volcanology and Geothermal Research, v. 140, p. 217–240.

Wallace, P.J., and Edmonds, M., 2011, The Sulfur Budget in Magmas: Evidence from Melt Inclusions, Submarine Glasses, and Volcanic Gas Emissions: Reviews in Mineralogy and Geochemistry, v. 73, p. 215–246.

White, R.S., 1997, Rift-Plume Interaction in the North Atlantic: Philosophical Transactions: Mathematical, Physical and Engineering Sciences, v. 355, p. 319–339.

Wolfe, C.J., Bjarnason, I.T., VanDecar, J.C., and Solomon, S.C., 1997, Seismic structure of the Iceland mantle plume: Nature, v. 385, p. 245–247.